

1 **Genomic dissection of 43 serum urate-associated loci provides**  
2 **multiple insights into molecular mechanisms of urate control.**

3

4 James Boocock<sup>1,2¶</sup>, Megan Leask<sup>1¶</sup>, Yukinori Okada<sup>3,4</sup>, Asian Genetic Epidemiology  
5 Network (AGEN) Consortium, Hirotaka Matsuo<sup>5</sup>, Yusuke Kawamura<sup>5</sup>, Yongyong  
6 Shi<sup>6</sup>, Changgui Li<sup>7</sup>, David B Mount<sup>8,9</sup>, Asim K Mandal<sup>8</sup>, Weiqing Wang<sup>10</sup>, Murray  
7 Cadzow<sup>1</sup>, Anna L Gosling<sup>1</sup>, Tanya J Major<sup>1</sup>, Julia A Horsfield<sup>11</sup>, Hyon K Choi<sup>12</sup>,  
8 Tayaza Fadason<sup>13</sup>, Justin O’Sullivan<sup>13</sup>, Eli A Stahl<sup>10&</sup>, Tony R Merriman<sup>1\*&</sup>

9

10 <sup>1</sup> Department of Biochemistry, Biomedical Sciences, University of Otago, Dunedin,  
11 New Zealand

12 <sup>2</sup> Department of Human Genetics, David Geffen School of Medicine at UCLA, Los  
13 Angeles, CA, USA

14 <sup>3</sup> Department of Statistical Genetics, Osaka University Graduate School of Medicine,  
15 Osaka, Japan

16 <sup>4</sup> Laboratory of Statistical Immunology, Immunology Frontier Research Center (WPI-  
17 IFReC), Osaka University, Suita, Japan

18 <sup>5</sup> Department of Integrative Physiology and Bio-Nano Medicine, National Defense  
19 Medical College, Tokorozawa, Saitama, Japan

20 <sup>6</sup> Bio-X Institutes, Key Laboratory for the Genetics of Developmental and  
21 Neuropsychiatric Disorders (Ministry of Education), Shanghai Jiao Tong University,  
22 Shanghai, People's Republic of China

23 <sup>7</sup> The Department of Endocrinology and Metabolism, The Affiliated Hospital of  
24 Qingdao University, Qingdao, People's Republic of China

25 <sup>8</sup> Renal Division, Brigham and Women’s Hospital, Harvard Medical School, Boston  
26 MA

27 <sup>9</sup> Renal Division, VA Boston Healthcare System, Harvard Medical School, Boston MA

28 <sup>10</sup> Department of Genetics and Genomic Sciences, Icahn Institute of Genomics and  
29 Multiscale Biology, New York, New York

30 <sup>11</sup> Department of Pathology, Otago Medical School, University of Otago, Dunedin,  
31 New Zealand

32 <sup>12</sup> Division of Rheumatology, Allergy and Immunology, Massachusetts General  
33 Hospital, Harvard Medical School, Boston, Massachusetts, United States of America

34 <sup>13</sup> Liggins Institute, University of Auckland, Auckland, New Zealand

35 \* Corresponding author

36 Email: [tony.merriman@otago.ac.nz](mailto:tony.merriman@otago.ac.nz)

37 ¶ These authors contributed equally to the work

38 & These authors contributed equally to the work

39

40

41

42

43

44

45

46

47

48

49

50

51

52

53

54

55

56

57

58

59

60

61

62

63

64

65

66

67

68

## 69 **Abstract**

70 Serum urate is the end-product of purine metabolism. Elevated serum urate is causal of  
71 gout and a predictor of renal disease, cardiovascular disease and other metabolic  
72 conditions. Genome-wide association studies (GWAS) have reported dozens of loci  
73 associated with serum urate control, however there has been little progress in  
74 understanding the molecular basis of the associated loci. Here we employed trans-  
75 ancestral meta-analysis using data from European and East Asian populations to  
76 identify ten new loci for serum urate levels. Genome-wide colocalization with *cis*-  
77 expression quantitative trait loci (eQTL) identified a further five new loci. By *cis*- and  
78 *trans*-eQTL colocalization analysis we identified 24 and 20 genes respectively where  
79 the causal eQTL variant has a high likelihood that it is shared with the serum urate-  
80 associated locus. One new locus identified was *SLC22A9* that encodes organic anion  
81 transporter 7 (OAT7). We demonstrate that OAT7 is a very weak urate-butyrates  
82 exchanger. Newly implicated genes identified in the eQTL analysis include those  
83 encoding proteins that make up the dystrophin complex, a scaffold for signaling  
84 proteins and transporters at the cell membrane; *MLXIP* that, with the previously  
85 identified *MLXIPL*, is a transcription factor that may regulate serum urate via the  
86 pentose-phosphate pathway; and *MRPS7* and *IDH2* that encode proteins necessary for  
87 mitochondrial function. Trans-ancestral functional fine-mapping identified six loci  
88 (*RREB1*, *INHBC*, *HLF*, *UBE2Q2*, *SFMBT1*, *HNF4G*) with colocalized eQTL that  
89 contained putative causal SNPs (posterior probability of causality > 0.8). This  
90 systematic analysis of serum urate GWAS loci has identified candidate causal genes at  
91 19 loci and a network of previously unidentified genes likely involved in control of  
92 serum urate levels, further illuminating the molecular mechanisms of urate control.

93

## 94 **Author Summary**

95 High serum urate is a prerequisite for gout and a risk factor for metabolic disease.  
96 Previous GWAS have identified numerous loci that are associated with serum urate  
97 control, however, only a small handful of these loci have known molecular  
98 consequences. The majority of loci are within the non-coding regions of the genome  
99 and therefore it is difficult to ascertain how these variants might influence serum urate  
100 levels without tangible links to gene expression and / or protein function. We have  
101 applied a novel bioinformatic pipeline where we combined population-specific GWAS

102 data with gene expression and genome connectivity information to identify putative  
103 causal genes for serum urate associated loci. Overall, we identified 15 novel serum  
104 urate loci and show that these loci along with previously identified loci are linked to  
105 the expression of 44 genes. We show that some of the variants within these loci have  
106 strong predicted regulatory function which can be further tested in functional analyses.  
107 This study expands on previous GWAS by identifying further loci implicated in serum  
108 urate control and new causal mechanisms supported by gene expression changes.

## 109 **Introduction**

110 Elevated serum urate (hyperuricemia) is causal of gout, an inflammatory arthritis  
111 increasing in prevalence world-wide [1, 2]. Monosodium urate crystals which form in  
112 hyperuricemic individuals can activate the NLRP3-inflammasome of resident  
113 macrophages to mediate an IL-1 $\beta$ -stimulated gout flare [3]. Long established genome-  
114 wide association studies (GWAS) [4, 5] have reported 28 loci associated with serum  
115 urate levels in European and East Asian sample sets with a more recent study reporting  
116 an additional 8 loci [6]. The loci of strongest effect are dominated by renal and gut  
117 transporters of urate, with two loci (*SLC2A9* and *ABCG2*) together explaining up to 5%  
118 of variance in serum urate levels in Europeans [4]. Most of these 36 loci also associate  
119 with gout in multiple ancestral groups [4, 7-9]. There has, however, been little progress  
120 on understanding the molecular basis of the association for the various loci. Probable  
121 causal genes have been identified at only about one fifth of the 36 loci [10-12], with  
122 strong evidence for causality for variants identified at *ABCG2* (*rs2231142*; Q141K) and  
123 *PDZK1* (*rs1967017*) [11, 13-17].

124

125 There have also been a number of recent improvements to the resources and analytical  
126 techniques that can be applied to the summary statistics of GWAS. Differences in  
127 underlying linkage disequilibrium (LD) structure between ancestral groups can be  
128 leveraged to amplify signal of association at shared causal variants [18, 19]. The  
129 epigenomics roadmap and ENCODE projects have generated a large resource of cell-  
130 and organ-specific regulatory regions [20, 21]. This information can be used to discover  
131 the cell-type specific regulatory regions that are known to be overrepresented in the  
132 heritability of a typical complex trait. Variants in regulatory regions identified by the  
133 epigenomics roadmap and ENCODE can be further analysed with functional annotation  
134 fine-mapping tools to identify candidate causal variants. Once credible sets of causal  
135 variants have been identified, expression quantitative trait loci (eQTL) sample sets (e.g.

136 GTEx [22]) can be used to translate from causal variants to affected genes, thus  
137 informing the design of functional experiments for insights into molecular pathogenic  
138 pathways. Since sample sizes for eQTL studies are relatively modest (<1000),  
139 colocalization analyses of GWAS and eQTL data have remained primarily focused on  
140 *cis*-eQTL. However, recent methods that integrate high resolution genomic interaction  
141 data with eQTL data can reduce the number of *trans*-eQTL investigated substantially  
142 [23, 24], although a limitation of this filtering approach is that it excludes *trans*-eQTL  
143 not mediated by genomic interactions [25]. Despite this limitation integrating genomics  
144 interaction-filtered *trans*-eQTL signals with GWAS allows expansion of our view of  
145 how GWAS associations underpin gene expression [24].

146

147 In this study, we integrated these analytical approaches with the summary statistics of  
148 two serum urate GWAS from European and East Asian individuals [4, 5]. By meta-  
149 analysis and colocalization analysis of serum urate and eQTL signals we identified 15  
150 new serum urate loci, identified 44 candidate causal genes connected to 25 loci,  
151 revealed the cell types that are enriched in serum urate heritability, and used this  
152 functional information to identify credible sets of causal variants using trans-ancestral  
153 fine-mapping.

154

## 155 **Results**

156 *Trans-ancestral meta-analysis identifies 10 new loci associated with serum urate levels*

157 The analysis approach for this study is summarised in Figure 1. *Z*-scores were imputed  
158 into the European [4] and East Asian [5] summary statistics using reference haplotypes  
159 from the Phase 3 1000 Genomes release and combined by meta-analysis (Figures 2 and  
160 S1). Study-specific results revealed three new loci at Chromosome 11 in the East Asian  
161 sample set (Chr11, 63.2-67.2Mb, *SLC22A9*, *PLA2G16*, *AIP*) in addition to those  
162 reported as genome-wide significant in the original GWAS [5] (Table 1; Figures 2, S2).  
163 All loci reported in the original GWAS reports [4, 5] were also detected in the trans-  
164 ancestral meta-analysis. However, the separate signals at *SLC22A11* and *SLC22A12*  
165 (Chr11, 64.4Mb) reported by Köttgen *et al.* [4] are reported as one signal in the trans-  
166 ancestral meta-analysis and an additional signal was detected at Chr11 65.4Mb (*RELA*).  
167 The trans-ancestral meta-analysis identified seven new loci (Chr4, 81.2Mb, *FGF5*;  
168 Chr5, 40.0Mb, *LINC00603*; Chr6, 32.7Mb, *HLA-DQB1*; Chr9, 33.2Mb, *B4GALT1*;  
169 Chr10, 60.3Mb, *BICC1*; Chr11, 63.9Mb, *FLRT1*; Chr11, 119.2Mb, *USP2*) (Figures 2

170 and S3). Of the ten new loci identified (seven from the trans-ancestral meta-analysis  
171 and three in the East Asian-specific analysis), five mapped within an extended Chr11  
172 locus (63.2-67.2Mb) that encompassed the previously identified *SLC22A11*, *SLC22A12*  
173 and *OVOLI / RELA* loci [4, 5]. In the East Asian GWAS, the peak marker falls outside  
174 the *RELA* locus (Figure S4). On closer inspection of the association signal from the  
175 region within and surrounding the *RELA* locus it is clear that the causal variants in the  
176 East Asian population are not the same as in the European population (Figure S4). On  
177 Chr6, given the association of the *HLA-DQB1* locus with T-cell-mediated  
178 autoimmunity [26] we also investigated if the lead *HLA-DQB1* SNP (*rs2858330*) was  
179 associated with other phenotypes using GWAS Central ([www.gwascentral.org](http://www.gwascentral.org)). There  
180 were no reported associations at  $P < 0.001$ , indicating that the *HLA-DQB1* signal in the  
181 serum urate GWAS is distinct from the association of this region with autoimmunity.  
182 The 35 loci found in Europeans explain 6.9% of variance in age and sex-adjusted serum  
183 urate levels. In summary, a total of 38 loci associated with serum urate concentration  
184 at a genome-wide level of significance were identified by this analysis.

185

186

187

188

189

190

191

192

193

194

195

196

197

198

199 Table 1. SNPs associated with serum urate concentrations by meta-analysis individuals of European and East Asian ancestry.

SNP	Chr: bp	Closest gene	A1 <sup>1</sup>	A2	Freq. A1 EUR	Freq. A1 EAS	$\beta_{\text{Köngens}}^2$ se, <i>P</i>	$\beta_{\text{Okada}}$ se, <i>P</i>	$\beta_{\text{Meta}}$ se, <i>P</i>	% var <sup>6</sup>				
<b>Previously reported loci (Köttgen <i>et al.</i>)</b>														
rs1471633	1: 145723739	<i>PDZK1</i>	A	C	0.49	0.84	0.061, 0.005, 1.5E-29	0.047, 0.023, 0.045	0.060, 0.005, 8.9E-29	0.11				
rs11264341	1: 155151493	<i>TRIM46</i>	C	T	0.59	0.31	-0.048, 0.006, 3.2E-16	-0.056, 0.019, 2.7E-03	-0.049, 0.006, 4.1E-18	0.07				
rs1260326	2: 27730940	<i>GCKR</i>	T	C	0.41	0.48	0.077, 0.006, 1.3E-44	0.052, 0.013, 1.0E-04	0.073, 0.005, 1.1E-46	0.17				
rs17050272	2: 121306440	<i>INHBB</i>	G	A	0.55	0.54	-0.037, 0.006, 1.2E-09	-0.035, 0.014, 0.014	-0.037, 0.006, 5.7E-11	0.04				
rs11894371	2: 148575872	<i>ACVR2A</i>	A	C	0.67	0.54	-0.034, 0.006, 4.5E-09	-0.004, 0.013, 0.76	-0.029, 0.005, 4.0E-08	0.03				
rs6770152	3: 53100214	<i>SFMBT1</i>	G	T	0.41	0.60	0.048, 0.006, 9.1E-18	0.022, 0.014, 0.14	0.045, 0.005, 2.0E-17	0.07				
rs11722228	4: 9915741	<i>SLC2A9</i>	C	T	0.65	0.73	0.206, 0.006, 6.9E-294	0.183, 0.014, 1.2E-36	0.203, 0.005, 0	3.10				
rs4148155	4: 89054667	<i>ABCG2</i>	A	G	0.91	0.71	-0.221, 0.009, 3.6E-129	-0.168, 0.015, 2.3E-30	-0.206, 0.008, 1.7E-157	0.51				
rs17632159	5: 72431482	<i>TMEM171</i>	G	C	0.71	0.74	0.038, 0.006, 3.4E-10	0.039, 0.015, 9.4E-03	0.028, 0.006, 1.1E-11	0.04				
rs675209	6: 7102084	<i>RREB1</i>	T	C	0.27	0.91	0.063, 0.006, 5.3E-24	0.043, 0.026, 0.10	0.062, 0.006, 4.0E-23	0.10				
rs1165213	6: 25799676	<i>SLC17A1</i>	G	A	0.44	0.18	-0.094, 0.005, 3.8E-66	-0.070, 0.018, 8.9E-05	-0.080, 0.005, 4.5E-67	0.26				
rs729761	6: 43804571	<i>VEGFA</i>	T	G	0.27	0.13	-0.046, 0.006, 2.0E-13	-0.022, 0.020, 0.27	-0.044, 0.006, 7.6E-13	0.05				
rs1178977	7: 72857049	<i>BAZ1B</i>	A	G	0.81	0.90	0.050, 0.007, 4.4E-13	0.049, 0.022, 2.5E-03	0.050, 0.007, 5.1E-14	0.05				
rs17786744	8: 23777006	<i>STC1</i>	A	G	0.57	0.65	-0.031, 0.005, 1.6E-08	-0.014, 0.015, 0.37	-0.029, 0.005, 3.1E-08	0.03				
rs2941484	8: 76478768	<i>HNF4G</i>	C	T	0.57	0.70	0.049, 0.006, 5.4E-19	0.049, 0.013, 3.1E-04	0.049, 0.005, 7.9E-22	0.07				
rs10994856	10: 52645248	<i>AICF</i>	G	A	0.80	0.95	0.053, 0.007, 2.3E-13	0.033, 0.032, 0.30	0.052, 0.007, 1.1E-12	0.06				
rs1171617	10: 61467182	<i>SLC16A9</i>	G	T	0.24	0.001	-0.073, 0.007, 2.4E-25	-	-	0.12				
rs10897518	11: 64360705	<i>SLC22A12</i>	C	T	0.29	0.78	0.070, 0.006, 1.2E-33	0.249, 0.018, 2.9E-45	0.088, 0.006, 5.2E-63	0.13				
rs12289836	11: 65436888	<i>RELA</i>	A	G	0.65	0.78	-0.044, 0.006, 3.5E-15	-0.068, 0.020, 6.1E-04	-0.046, 0.005, 8.9E-18	0.05				
rs3741414	12: 57844049	<i>INHBC</i>	C	T	0.81	0.93	-0.071, 0.007, 8.3E-24	-0.030, 0.025, 0.24	-0.068, 0.007, 4.1E-22	0.10				
rs653178	12: 112007756	<i>ATXN2</i>	C	T	0.47	0.003	0.036, 0.005, 2.0E-11	-	-	0.04				
rs1976748	15: 76160951	<i>UBE2Q2</i>	A	G	0.50	0.37	-0.037, 0.006, 1.3E-11	-0.028, 0.014, 0.046	-0.036, 0.005, 2.7E-12	0.05				
rs6598541	15: 99271135	<i>IGF1R</i>	A	G	0.35	0.43	0.044, 0.006, 2.7E-14	0.049, 0.014, 3.1E-04	0.044, 0.005, 3.7E-17	0.04				
rs33063	16: 69640217	<i>NFAT5</i>	A	G	0.14	0.08	0.042, 0.008, 6.1E-08	0.096, 0.026, 1.7E-04	0.046, 0.007, 9.9E-11	0.03				
rs11150189	16: 79734227	<i>MAF</i>	A	G	0.65	0.72	0.032, 0.006, 2.4E-08	0.054, 0.014, 2.1E-04	0.035, 0.005, 4.0E-11	0.03				
rs7224610	17: 53364788	<i>HLF</i>	C	A	0.43	0.14	0.038, 0.006, 4.3E-12	0.030, 0.017, 0.083	0.037, 0.005, 1.9E-12	0.04				
rs9895661	17: 59456589	<i>BCAS3</i>	C	T	0.19	0.53	-0.045, 0.008, 1.7E-09	-0.053, 0.015, 6.1E-04	-0.047, 0.007, 5.3E-12	0.04				
rs164009	17: 74283669	<i>OR1CH2</i>	A	G	0.62	0.35	0.029, 0.006, 2.1E-07	0.027, 0.014, 0.065	0.028, 0.005, 4.0E-08	0.02				
<b>New loci</b>														
rs11099098	4: 81169912	<i>FGF5</i>	G	T	0.72	0.61	0.033, 0.006, 1.4E-07	0.039, 0.014, 5.5E-03	0.034, 0.006, 2.9E-09	0.03	$\beta_{\text{Kanaji}}$ se, <i>P</i>	$\text{OR}_{\text{GoutUKBB}}$ se, <i>P</i> <sup>3</sup>	$\text{OR}_{\text{GoutJapan}}$ se, <i>P</i>	$\text{OR}_{\text{GoutChina}}$ se, <i>P</i>
rs7706096	5: 39994900	<i>LINC00603</i>	G	A	0.41	0.49	0.028, 0.005, 3.8E-07	0.029, 0.013, 0.031	0.028, 0.005, 3.5E-08	0.02	0.025, 0.004, 2.8E-08	1.03, 0.019, 0.14	1.11, 0.065, 0.12	-
rs2858330	6: 32658715	<i>HLA-DOB1</i>	T	C	0.49	0.25	0.026, 0.005, 1.9E-06	0.043, 0.015, 5.4E-03	0.027, 0.005, 4.2E-08	0.02	0.005, 0.004, 0.23	1.00, 0.017, 0.90	1.00, 0.061, 0.97	0.89, 0.098, 0.24
rs10813960	9: 33180362	<i>B4GALT1</i>	C	T	0.73	0.46	0.033, 0.006, 1.9E-07	0.040, 0.013, 2.9E-03	0.035, 0.006, 2.3E-09	0.03	- <sup>7</sup>	1.01, 0.017, 0.46	- <sup>5</sup>	-
rs1649053	10: 60321487	<i>BICC1</i>	T	C	0.61	0.77	-0.027, 0.006, 9.8E-07	-0.051, 0.016, 1.6E-03	-0.029, 0.005, 8.9E-09	0.02	0.017, 0.004, 5.8E-05	1.04, 0.019, 0.070	0.90, 0.066, 0.10	1.04, 0.096, 0.68
rs11231463	11: 63184455	<i>SLC22A9</i>	A	G	0.99	0.94	-	0.312, 0.029, 4.3E-27	-	0.80	-0.020, 0.005, 5.3E-05	0.95, 0.017, 1.6E-03	0.99, 0.095, 0.92	0.97, 0.112, 0.83
rs7928514	11: 63360114	<i>PLA2G16</i>	G	A	0.90	0.90	- <sup>3</sup>	0.115, 0.021, 5.5E-10	-	0.17	0.207, 0.009, 6.6E-123	1.05, 0.098, 0.61	1.39, 0.133, 0.013	1.41, 0.282, 0.22
rs641811	11: 63869596	<i>FLRT1</i>	G	A	0.82	0.78	0.030, 0.007, 7.7E-06	0.072, 0.014, 5.9E-07	0.037, 0.006, 1.0E-09	0.02	0.086, 0.006, 3.8E-54	0.98, 0.027, 0.47	1.31, 0.082, 9.7E-04	-
rs11227805	11: 67246757	<i>AIP</i>	C	T	0.79	0.88	- <sup>4</sup>	0.141, 0.023, 5.5E-10	-	0.25	0.079, 0.004, 5.0E-70	1.07, 0.021, 1.2E-03	0.99, 0.066, 0.82	-
rs2195525	11: 119235404	<i>USP2</i>	C	T	0.46	0.17	0.031, 0.006, 5.3E-08	0.035, 0.017, 0.040	0.031, 0.005, 6.3E-09	0.03	0.085, 0.007, 2.6E-34	0.97, 0.021, 0.21	1.01, 0.101, 0.89	-
<b>Independent signals</b>														
rs10939614	4: 9926613	<i>SLC2A9</i>	T	C	0.34	0.10	0.179, 0.008, 9.2E-118	-	-	0.90	0.013, 0.005, 0.019	1.06, 0.017, 1.7E-03	1.12, 0.078, 0.13	-
rs4447861	4: 9953940	<i>SLC2A9</i>	C	T	0.59	0.91	0.143, 0.009, 8.2E-57	-	-	0.50	0.013, 0.005, 0.019	1.06, 0.017, 1.7E-03	1.12, 0.078, 0.13	-
rs12499240	4: 10103890	<i>SLC2A9</i>	T	C	0.27	0.38	0.062, 0.007, 3.12E-19	-	-	0.07	1.24, 0.017, 1.7E-34	1.30, 0.103, 0.013	1.37, 0.135, 0.021	-
rs4698031	4: 10315921	<i>SLC2A9</i>	A	G	0.82	0.87	0.121, 0.009, 4.18E-18	-	-	0.38	1.15, 0.017, 3.5E-15	0.78, 0.116, 0.031	0.89, 0.149, 0.42	-
rs2622629	4: 89094064	<i>ABCG2</i>	T	C	0.69	0.44	-0.056, 0.006, 3.5E-22	-	-	0.08	0.95, 0.019, 7.5E-03	1.09, 0.063, 0.19	0.87, 0.100, 0.18	-
rs575416	5: 72437534	<i>TMEM171</i>	A	G	0.90	0.99	-0.045, 0.009, 7.7E-07	-	-	0.02	1.58, 0.024, 3.6E-78	1.09, 0.085, 0.33	1.45, 0.156, 0.017	-
rs1171606	10: 61434519	<i>SLC16A9</i>	G	A	0.72	0.40	-0.036, 0.006, 2.2E-08	-	-	0.03	0.90, 0.018, 3.9E-09	0.80, 0.063, 3.3E-04	0.96, 0.093, 0.64	-
rs2269730	11: 64423831	<i>SLC22A12</i>	G	A	0.80	0.55	-0.050, 0.007, 7.1E-14	-	-	0.05	0.90, 0.027, 1.4E-04	1.27, 0.18, 0.19	-	-
<b>Cis-eQTL co-localised loci</b>														
$\beta_{\text{Köngens}}^1$ se, <i>P</i>														

rs3815574	2: 169963330	<i>DHRS9</i>	A	C	0.52	0.37	0.025, 0.005, 4.0E-06	0.013, 0.016, 0.41	0.023, 0.005, 5.3E-06	0.02	0.000, 0.005, 0.98	1.06, 0.017, 8.1E-04	0.98, 0.067, 0.76	0.87, 0.095, 0.16
rs461660	5:34657025	<i>RAI14</i>	A	C	0.55	0.38	0.026, 0.006, 5.4E-06	0.007, 0.014, 0.63	0.023, 0.005, 1.4E-05	0.02	0.013, 0.005, 3.6E-03	1.07, 0.017, 1.0E-04	0.91, 0.065, 0.17	0.97, 0.099, 0.78
rs7953704	12: 121517820	<i>MLXIP</i>	A	G	0.47	0.51	-0.028, 0.006, 3.5E-07	-0.003, 0.013, 0.84	-0.024, 0.005, 2.1E-06	0.02	-0.017, 0.004, 3.3E-05	0.90, 0.017, 3.1E-09	0.90, 0.061, 0.091	0.90, 0.094, 0.27
rs8024386 <sup>5</sup>	15:90670526	<i>IDH2</i>	A	C	0.74	0.79	-0.029, 0.006, 3.9E-06	-0.018, 0.020, 0.37	-0.028, 0.006, 4.3E-06	0.02	-0.007, 0.006, 0.25	0.89, 0.020, 8.9E-09	0.89, 0.081, 0.16	1.10, 0.120, 0.44
rs4788878	17: 73260298	<i>MRPS7</i>	A	G	0.18	0.04	-0.034, 0.007, 2.4E-06	-0.000, 0.034, 0.99	-0.032, 0.007, 1.5E-05	0.02	0.006, 0.010, 0.57	0.95, 0.023, 0.027	1.10, 0.169, 0.57	0.75, 0.241, 0.22

200 <sup>1</sup> A1 is the effect allele

201 <sup>2</sup> Not identical to *Köttgen et al.* [4] or *Okada et al.* [5] *P* value. This *P* value is from z-score adjusted by LD-score intercept in both *Okada* and  
202 *Köttgen*.  $\beta$  in mg/dL.

203 <sup>3</sup> Age- and sex-adjusted. At the independent signals data were extracted directly from GWAS summary statistics with no modelling to determine  
204 whether or not the signals were independent with gout as outcome.

205 <sup>4</sup> A triallelic variant was removed during imputation.

206 <sup>5</sup> The variant was not imputed in the Japanese data set.

207 <sup>6</sup> Variance explained is estimated where possible using the European data set. The variance explained for the conditionally independent signals is  
208 estimated from the joint model. For all other loci, the marginal effects are used.

209 <sup>7</sup> *HLA-DQ* data were not reported by *Kanai et al.* [6]

210 <sup>8</sup> Surrogate rs7175469 was used in the Chinese gout data set –  $r^2 = 0.97$ ,  $D' = 1.0$ .

211

212

213

214

215

216

217

218

219

220

221



222 *Conditional analysis identifies 8 additional variants associated with serum urate*

223 Using the European summary statistics, a conditional and joint analysis was performed  
224 with the objective of identifying independent genetic effects. Conditional and joint  
225 analysis identified an additional four genome-wide significant associations at *SLC2A9*,  
226 and one at each of *ABCG2*, *TMEM171*, *SLC16A9* and *SLC22A11/A12* (Table 1). The  
227 conditional analysis was limited to four independent associations at each locus,  
228 therefore it remains possible that there are additional unidentified associations at these  
229 loci. In a joint model these four loci explained an additional 0.54% of the variance of  
230 age- and sex-adjusted serum urate levels (Table 1).

231

232 *Population-specific associations with serum urate levels*

233 LocusZoom plots from each population were visually compared to the trans-ancestral  
234 meta-analysis to identify population-specific and shared patterns of association. For 16  
235 loci (*ABCG2*, *B4GALT1*, *BCAS3*, *FGF5*, *BICCI1*, *HFN4G*, *IGF1R*, *INHBB*, *NFAT5*,  
236 *PDZK1*, *QRICH2*, *SLC16A9*, *SLC17A1*, *TMEM171*, *TRIM46*, *UBE2Q2*) the pattern of  
237 association was consistent between the East Asian and European GWAS suggesting  
238 strong similarity between the underlying haplotypic structure and casual variant(s)  
239 (Figure S5). The *MAF* locus contains two association signals in the East Asian  
240 population, one that is shared with the European population and one that is specific to  
241 the East Asian population (Figure S6) [12]. The lead SNP for the East Asian population  
242 is *rs889472*; this variant is common in both European (C-allele = 0.38) and East Asian  
243 (C-allele = 0.60) individuals from the 1000 Genomes Project yet there is no serum urate  
244 association signal in the European population. Two other East Asian-specific signals  
245 were identified on chromosome 11 near the *SLC22A9* and *PLA2G16* genes in addition  
246 to the previously mentioned East Asian-specific signal at the *RELA* locus. These loci,  
247 in combination with the conditionally independent and trans-ancestral associations,  
248 mean that there are seven independent associations on chromosome 11 between 63.1Mb  
249 and 67.3Mb.

250

251 *Cis-eQTL colocalization analysis identifies 24 candidate causal genes at 19 serum*  
252 *urate loci.*

253 To connect the serum urate associations with the genes they influence, we utilised  
254 publicly available expression data provided by the GTEx consortium and performed  
255 colocalization with COLOC [27] (Figure S7 and Table 2). This method attempts to  
256 identify whether the causal variant is the same in both the eQTL and GWAS signal

257 indicating a putative causal mechanism, whereby the variant alters gene expression  
 258 (transcript levels) and expression influences the trait – in this case serum urate levels.  
 259 This approach provides further support for the loci identified by the trans-ancestral  
 260 meta-analysis by linking the serum urate signals into the biological process of gene  
 261 regulation. For 19 of the serum urate GWAS loci strong evidence for colocalization  
 262 (PPC > 0.8) was seen with 24 *cis*-eQTL (Table 2; Figure S7). The 19 loci included five  
 263 loci identified by inclusion of sub-genome-wide significant GWAS loci in the analysis  
 264 (*DHRS9*, *RAI14*, *MLXIP*, *IDH2*, *MRPS7*). For 11 of the previously identified Köttgen  
 265 *et al.* [4] GWAS loci there are colocalized *cis*-eQTL (*PDZK1*, *TRIM46*, *INHBB*,  
 266 *SFMBT1*, *BAZ1B*, *SLC16A9*, *INHBC*, *UBE2Q2*, *IGF1R*, *MAF*, *QRICH2*). Of the ten  
 267 new loci discovered as genome-wide significant in the trans-ancestral meta-analysis  
 268 colocalized eQTL were identified at three loci (*HLA-DQB1*, *B4GALT1*, *RELA*).

269

270 **Table 2. Serum urate associated loci with colocalized GTEx eQTL.**

271

Locus	Lead GWAS variant	Colocalized eQTL gene	PPC <sup>1</sup>	Tissue(s)	Direction (allele, $\beta_{SU}$ mg/dL, $\beta$ Expression, $P$ Expression)
Cis-eQTL (genome-wide significant by trans-ancestral meta-analysis)					
<i>PDZK1</i>	rs1471633	<i>PDZK1</i>	0.98	colon - transverse, small intestine	A, 0.061, 0.58, 1.3E-11 (colon - transverse)
<i>TRIM46</i>	rs11264341	<i>MUC1</i>	0.93	adipose subcutaneous, artery aorta, esophagus mucosa, esophagus muscularis, testis, whole blood	T, -0.048, 0.34, 7.7E-16 (esophagus – mucosa)
		<i>GBAP1</i>	0.98	skin	T, -0.048, -0.35, 2.7E-08
		<i>FAM189B</i>	0.92	heart atrial appendage	T, -0.048, -0.23, 1.1E-05
<i>INHBB</i>	rs17050272	<i>INHBB</i>	0.80	lung	G, -0.037, 0.23, 2.2E-05
<i>SFMBT1</i>	rs6770152	<i>TMEM110</i>	0.86	adipose subcutaneous, skin	T, -0.048, 0.24, 1.1E-05 (adipose subcutaneous)
		<i>SFMBT1</i>	0.97	colon transverse	T, -0.048, 0.45, 1.9E-10
<i>HLA-DQB1</i>	rs2858330	<i>HLA-DQA2</i>	0.82	prostate	T, 0.026, -0.79, 2.8E-12
<i>BAZ1B</i>	rs1178977	<i>MLXIPL</i>	0.88	adipose visceral, transformed fibroblasts	T, 0.050, -0.48, 1.2E-08 (transformed fibroblasts)
<i>B4GALT1</i>	rs10813960	<i>B4GALT1</i>	0.81	EBV transformed lymphocytes, esophagus mucosa	T, -0.033, -0.47, 1.9E-04 (EBV transformed lymphocytes)
<i>SLC16A9</i>	rs1171617	<i>SLC16A9</i>	0.84	artery aorta, thyroid	T, 0.073, -0.28, 2.2E-06 (thyroid)
<i>RELA</i>	rs12289836	<i>OVOLI-ASI</i>	0.88	thyroid, caudate basal ganglia, cortex	A, -0.043, 0.55, 3.7E-06 (basal ganglia) <sup>2</sup>
<i>INHBC</i>	rs3741414	<i>R3HDM2</i>	0.84	transformed fibroblasts	T, -0.071, 0.21, 2.2E-05

<i>UBE2Q2</i>	rs1976748	<i>UBE2Q2</i>	0.91	dorsolateral prefrontal cortex	A, -0.037, -0.10, 8.5E-30
<i>IGF1R</i>	rs6598541	<i>IGF1R</i>	0.83	heart left ventricle	A, 0.044, -0.33, 1.7E-07
<i>MAF</i>	rs11150189	<i>MAFTRR</i>	0.84	colon sigmoid, pancreas	A, 0.032, 0.52, 1.2E-05 (colon sigmoid)
<i>QRICH2</i>	rs164009	<i>UBALD2</i>	0.90	esophagus muscularis, caudate basal ganglia, whole blood	A, 0.029, 0.23, 7.7E-07 (esophagus muscularis)
		<i>PRPSAP1</i>	0.85	anterior cingulate cortex	A, 0.029, 0.62, 1.7E-06
<b>Cis-eQTL (sub genome-wide significant by trans-ancestral meta-analysis)</b>					
<i>DHRS9</i>	rs3815574	<i>DHRS9</i>	0.83	whole blood	A, 0.024, -0.30, 1.7E-26
<i>RAI14</i>	rs461660	<i>RAI14</i>	0.83	thyroid	A, 0.026, 0.24, 3.5E-07
<i>MLXIP</i>	rs7953704	<i>MLXIP</i>	0.83	small intestine	A, -0.028, 0.48, 9.6E-07
<i>IDH2</i>	rs8024386	<i>IDH2</i>	0.87	atrial appendage	A, -0.029, 0.35, 1.1E-06
<i>MRPS7</i>	rs4788878	<i>GGA3</i> <i>MRPS7</i>	0.83 0.87	thyroid dorsolateral prefrontal cortex, colon transverse, transformed fibroblasts, pancreas	A, -0.034, 0.23, 1.9E-08 A, -0.034, 0.07, 2.5E-12 (dorsolateral prefrontal cortex)
<b>Trans-eQTL</b>					
<i>NFAT5</i>	rs33063	<i>AIF1L</i> <i>CACNA2D3</i> <i>STIM1</i>	0.92 0.99 0.99	brain substantia nigra basal ganglia basal ganglia	A, 0.042, 0.39, 1.9E-05 A, 0.042, 0.23, 4.2E-06 A, 0.042, 0.26, 5.6E-07
<i>SLC16A9</i>	rs1171617	<i>ANKS1B</i> <i>DSCAM</i>	0.98 0.98	testis brain hypothalamus	T, 0.073, 0.17, 1.8E-05 T, 0.073, 0.51, 1.9E-05
<i>BAZ1B</i>	rs1178977	<i>RNF24</i>	0.98	brain cortex	A, 0.050, -0.43, 1.3E-05
<i>QRICH2</i>	rs164009	<i>PPP3R1</i>	0.98	heart left ventricle	A, 0.029, -0.18, 7.0E-06
<i>INHBB</i>	rs17050272	<i>CHAC2</i> <i>ZNF804A</i>	0.97 0.99	basal ganglia brain anterior cingulate cortex	A, 0.037, -0.36, 1.3E-05 A, 0.037, 0.23, 1.1E-05
<i>UBE2Q2</i>	rs1976748	<i>COL11A1</i>	0.95	colon transverse	A, -0.037, 0.23, 6.0E-06
<i>HNF4G</i>	rs2941484	<i>CSMD2</i>	0.99	brain cerebellum	T, 0.049, -0.40, 5.2E-06
<i>INHBC</i>	rs3741414	<i>SPIN1</i>	0.98	brain frontal cortex	T, -0.071, -0.22, 1.7E-05
<i>DHRS9</i>	rs3815574	<i>JHDM1D</i>	0.94	brain hippocampus	A, 0.024, 0.32, 1.3E-05
<i>IDH2</i>	rs8024386	<i>MAPK6</i> <i>ZBTB20</i>	0.86 0.89	brain amygdala testis	A, -0.029, -0.32, 1.2E-04 A, -0.029, 0.10, 1.8E-05
<i>RREB1</i>	rs675209	<i>UTRN</i>	0.99	brain putamen basal ganglia	T, 0.063, 0.35, 2.1E-05
<i>HLF</i>	rs7224610	<i>DMD</i>	0.94	brain nucleus accumbens basal ganglia	A, -0.038, -0.36, 1.9E-05
<i>VEGFA</i>	rs729761	<i>CLPS</i>	1.00	brain cerebellar hemisphere	T, -0.046, -0.59, 3.8E-06
<i>MLXIP</i>	rs7953704	<i>NDUFA12</i>	0.95	brain putamen basal ganglia	A, -0.028, -0.32, 2.0E-05
<i>BCAS3</i>	rs9895661	<i>TMEM117</i>	0.99	prostate	T, 0.045, 0.48, 3.9E-06

272 <sup>1</sup> Posterior probability of colocalization (PPC)

273 <sup>2</sup> Data from proxy variant rs642803.

274

275

276 *CoDeS3D analysis integration with GTEx and colocalization for identification of trans-*  
277 *eQTL*

278 To identify candidate causal genes that represent *trans*-eQTL, we pre-screened for  
279 SNP-gene physical connectivity using the CoDeS3D algorithm and then tested for  
280 colocalization with serum urate GWAS signals (Table 2). This identified 20 *trans*-  
281 eQTL signals that co-localized (PPC > 0.8) with 15 GWAS loci (Figure S7). Of the 20  
282 genes with colocalized *trans*-eQTL we identified, only two had evidence within the  
283 gene ( $P < 5 \times 10^{-04}$ ) for a signal of association with serum urate by GWAS (Figure S8)  
284 – *UTRN* in the Köttgen *et al.* dataset (lead variant *rs4896735*,  $P = 2 \times 10^{-04}$ ) and *DMD*  
285 (*rs1718043*;  $P = 9 \times 10^{-05}$ ) in the Kanai *et al.* [6] dataset. The *DMD* and *UTRN* genes  
286 encode components of the dystrophin complex. Notably, *MAPK6* (also known as  
287 *ERK3*) and a *trans*-eQTL identified at the *IDH2* locus has a signal of association with  
288 serum urate levels in response to allopurinol in gout by GWAS (*rs62015197*,  $P = 8 \times$   
289  $10^{-07}$ ) [28].

290

291 Nine serum urate loci (*SLC16A9*, *BAZ1B*, *QRICH2*, *UBE2Q2*, *INHBB*, *INHBC*,  
292 *DHRS9*, *MLXIP*, *IDH2*) exhibited both *cis*- and *trans*-eQTL of which the latter three  
293 had been identified by the genome-wide colocalization analysis. At *SLC16A9*, the  
294 signal is different between the *cis*- and *trans*-eQTL (Figure S7), with all of the GWAS  
295 signal present in the *cis*-eQTL whereas only the signal associated with the lead GWAS  
296 SNP was evident in the *trans*-eQTL. Also, at *SLC16A9* there was a second *cis*-eQTL  
297 over *CCDC6* that was weakly associated with serum urate levels. Differential *cis*- and  
298 *trans*-eQTL signals are reminiscent of the situation at the serum urate-associated *cis*-  
299 and *trans*-eQTL signals at the *MAFTRR* locus [12].

300

301 *Replication in Kanai et al.*

302 While this work was being finalized a serum urate GWAS comprising 109,029  
303 Japanese individuals (of whom 18,519 over-lapped with the Okada *et al.* [5] study) was  
304 published [6] allowing an opportunity to replicate our findings. Seven of the 15 new  
305 loci we identified replicated ( $P < 0.003$ ) in the Kanai *et al.* [6] study (Table 1). The  
306 replicated loci included two (*FGF5* and *BICC1*) of the total 27 genome-wide significant  
307 signals reported by Kanai *et al.* – of the remaining 25 loci identified by Kanai *et al.* [6]  
308 17 had previously been reported by others [4, 29, 30] and eight new (the gene containing  
309 the lead SNP or the flanking genes at each locus: *RNF115* (*rs12123298*), *USP23*

310 (*rs7570707*), *UNCX* (*rs4724828*), *TP53INP1* (*rs7835379*), *EMX2/RAB11F1P2*  
311 (*rs1886603*), *SBF2* (*rs2220970*), *MPPED2/DCDC5* (*rs963837*), *GNAS* (*rs6026578*)).

312

### 313 *Testing for association with gout*

314 To replicate the urate signals we tested the independent signals at eight existing loci,  
315 ten new loci with genome-wide significance in the trans-ancestral meta-analysis and  
316 five loci discovered by colocalization with eQTL (Table 1) for association with gout in  
317 European (UK Biobank) [31], Chinese [32] and Japanese [30] sample sets. The *BICCI1*,  
318 *FLRT1* and *USP2* loci replicated ( $P \leq 1.6 \times 10^{-03}$ ) in the European dataset in a  
319 directionally-consistent fashion (i.e. the urate-increasing allele associated with an  
320 increased risk of gout). The *SLC22A9* and *PLA2G16* loci replicated ( $P \leq 0.013$ ) in the  
321 Japanese dataset also in a directionally-consistent fashion. All eight additional variants  
322 identified in the European serum urate data set by conditional analysis (Table 1) were  
323 replicated ( $P \leq 3.3 \times 10^{-03}$ ), in the European gout data set. For the five loci identified  
324 by colocalization with eQTL, all replicated ( $P \leq 0.027$ ) in the European gout data set,  
325 with *IDH2* and *MLXIPL* at a genome-wide level of significance ( $P < 5.0 \times 10^{-08}$ ). All  
326 had an OR for gout consistent with the direction of effect on serum urate levels. None  
327 of these five loci were associated with gout in the Chinese or Japanese sample sets.

328

### 329 *Functional partitioning of the heritability of serum urate levels*

330 To understand the functional categories that contribute most to the heritability of serum  
331 urate level, we used LD score regression to functionally partition the SNP heritability  
332 of the European serum urate GWAS (Figures 3, S9; Table S1). Functional partitioning  
333 of serum urate SNP heritability according to cell type revealed significant enrichments  
334 in the kidney ( $P = 3.2 \times 10^{-08}$ ), the gastrointestinal tract ( $P = 5.2 \times 10^{-08}$ ), and the liver  
335 ( $P = 3.4 \times 10^{-03}$ ). A refined analysis of 218 functional annotations, which contribute to  
336 the larger cell type groups, revealed 11 significant annotations: four histone marks in  
337 the kidney H3K27ac ( $P = 1.2 \times 10^{-07}$ ), H3K9Ac ( $P = 1.5 \times 10^{-06}$ ), H3K4me3 ( $P = 9.6 \times$   
338  $10^{-0.6}$ ), and H3K4me1 ( $P = 2.5 \times 10^{-05}$ ) and two histone marks in the gastrointestinal  
339 tract - H3K27ac ( $P = 5.6 \times 10^{-06}$ ), and H3K4me1 ( $P = 4.8 \times 10^{-05}$ ). These histone marks  
340 are characteristic of transcriptional activation and consistent with active expression of  
341 nearby genes.

342

### 343 *Trans-ancestral functional fine-mapping identifies putative causal variants*

344 We sought to leverage both the functional enrichments and linkage disequilibrium  
 345 differences between the populations to identify candidate causal variants at each locus  
 346 associated with serum urate levels. To this end, we performed trans-ancestral fine-  
 347 mapping with PAINTOR using the kidney, gastrointestinal tract, and liver cell type  
 348 group annotations as functional priors. When analysing only the European GWAS the  
 349 90% causal credible sets had on average 129 SNPs. With the addition of the East Asian  
 350 GWAS data the set size reduced to an average of 56 SNPs, and functional annotations  
 351 reduced the average credible set size to 41. Of the 36 loci used in this analysis (the 28  
 352 reported by Köttgen *et al.* [4] and the ten new genome-wide significant loci reported  
 353 here, excluding *RELA* and *HLA-DQBI*), 14 loci had seven or fewer causal variants in  
 354 their 80% causal credible set (Tables 3, S3). The combination of both the functional  
 355 annotations and East Asian GWAS data significantly improves our ability to identify  
 356 the causal variants for loci associated with serum urate levels.

357

358 **Table 3. Putative credible causal SNP set identified with PAINTOR.**

Locus	Chr:pos	SNP ID	Posterior prob	European Z-score <sup>2</sup>	East Asian Z-score	Motifs changed (haploreg)
SLC2A9	4:9915741	rs11722228	1.000	-36.73	-12.67	None
SLC2A9	4:9946095	rs4697701	1.000	59.52	9.52	E2a, Mxi1
SLC2A9	4:9954660	rs11723382	1.000	38.02	7.24	Hmx, Nkx2
SLC2A9	4:9981997	rs13145758	1.000	-57.11	-2.66	Egr1, GCNF, HNF4
SLC2A9	4:9982330	rs13125646	1.000	-49.28	-2.66	None
ABCG2	4:88917735	rs17013705	1.000	4.44	5.10	Irf, TATA, TCF12
ABCG2	4:88944511	rs2725227	1.000	-7.22	-2.52	Gfi1, TCF11, MafG
ABCG2	4:88960528	rs2725217	1.000	-17.56	-9.73	CDP7, Dbx1, HNF1, Mef2, Pouf1, TATA
ABCG2	4:88973427	rs2725210	1.000	-15.27	-4.69	Fox, FoxA, FoxC1, FoxJ2, FoxF2, FoxK1, PLZF
ABCG2	4:88999222	rs2728126	1.000	-15.65	-8.72	EWRS1, FLI1
ABCG2	4:89052323	rs2231142	1.000	-24.26	-11.43	GR, Irf
ABCG2	4:89098731	rs9631715	1.000	15.34	7.24	GATA, SREBP
SLC17A1	6:25785295	rs6909187	1.000	15.65	-0.77	FoxC1, HDAC2, HMG-IY, Pou2F2
SLC17A1	6:25786993	rs3799344	1.000	15.36	2.10	Eomes, Pax6, TBX5
UBE2Q2	15:76194286	rs335685	1.000	5.25	0.13	CEBPB, DMRT1, FoxA, Nanog, Nkx6, Pou2F2, Pou3F4, STAT, TATA
SFMBT1	3:53092375	rs9870898	0.996	5.15	0.63	AhR, GR, HES1, HNF1, Pax4
SFMBT1	3:53026384	rs2564938	0.996	-6.86	-1.46	None
SFMBT1	3:53026714	rs2115779	0.996	5.38	1.63	Hsf, Ptf1b
SLC22A12	11:64333296	rs1783811	0.994	7.91	5.00	Mef2, TAL1, ZID
UBE2Q2	15:76160951	rs1976748	0.991	-6.78	-2.00	Arid3a, Sox, TCF4
AIP	11:67246757	rs11227805	0.991	NA <sup>1</sup>	6.22	None
SLC22A12	11:64358241	rs11602903	0.990	11.16	13.45	BAF155
SLC22A12	11:64387932	rs2277311	0.990	10.79	14.29	Hic1
SLC22A12	11:64338228	rs11231822	0.990	12.88	-2.62	CTCF, ERalphaA, Lmo2, Nanog
SLC22A12	11:64419217	rs502571	0.990	-8.41	-10.70	Mrg1, Hoxa9, TAL1
SLC22A12	11:64474752	rs2957564	0.990	-8.45	-10.94	GR, LUN1
SLC22A12	11:64622502	rs2007521	0.990	-1.50	-6.90	API, CTCF, Ets
SLC17A1	6:25798932	rs1165215	0.986	-16.73	-3.92	None
SLC17A1	6:26125342	rs129128	0.986	5.24	-0.09	None
SLC22A9	11:63170736	rs7925182	0.981	-1.26	-0.94	Barx1
USP2	11:119235404	rs2195525	0.978	5.46	2.06	API, Foxa, STAT
RREB1	6:7102084	rs675209	0.964	10.13	1.63	CCNT2, Ets, MZF1, NRSF, STAT, VDR, Zfp281, Zfp740
HNF4G	8:76401359	rs13264750	0.964	0.44	-2.78	Pou3f2
HLF	17:53364788	rs7224610	0.920	6.95	1.74	None
GCKR	2:27730940	rs1260326	0.868	14.00	3.89	NRSF



INHBC	12:57807114	rs540730	0.851	-9.44	0.75	None
SLC22A9	11:63859120	rs11231454	0.810	-0.31	10.01	GATA
SLC22A9	11:63171309	rs12281229	0.810	-1.01	-3.09	Cdx, Dbx1, Fox, FoxA, fOXc1, FoxD3, FoxF1, FoxI1, FoxJ1, Foxj2, FoxK1, FoxL1, Foxo, FoxP1, HDAC2, HNF1, Hlx1, HoxD8, Mef2, NF-Y, Ncx, Pbx-1, Pbx3, TATA

359 <sup>1</sup> At AIP

360 <sup>2</sup> Z-scores are reported because effect sizes are not available for imputed variants.

361

362 *SLC2A9* is a complex locus with a very strong effect on serum urate levels and multiple  
 363 independent genetic effects [33, 34]. A subset of the lead urate SNPs at *SLC2A9* with  
 364 PAINTOR posterior probabilities of 1.0 overlap putative regulatory elements (Tables  
 365 3, S4). One of these urate-associated variants at *SLC2A9*, *rs11723382*, is also among  
 366 the maximally-associated *cis*-eQTL variants for *RP11-448G15.1* (transformed  
 367 lymphocytes) (*RP11-448G15.1* is a lncRNA located within the second intron of  
 368 *SLC2A9*) and disrupts two predicted motifs Hmx and Nkx2 (Figure S10 and Table 3)  
 369 [35]. This eQTL was not identified in our COLOC analysis, however visual inspection  
 370 of the *RP11-448G15.1* eQTL and *SLC2A9* GWAS signal indicates that the signals  
 371 coincide and suggests *RP11-448G15.1* expression is likely important for serum urate  
 372 control.

373

374 At *SLC22A12 / NRXN2*, four of the seven putative causal variants (Table 3) are in LD  
 375 ( $R^2 > 0.6$ ) with the maximal *trans*-eQTL variant for *RNF169* identified by CoDeS3D.  
 376 Visual inspection of the *RNF169 trans*-eQTL and the serum urate signal at the  
 377 *SLC22A12 / NRXN2* locus indicates that these signals overlap (Figure S10). *rs2277311*,  
 378 an intronic variant located within *NRXN2*, is the most likely candidate of these variants  
 379 to have regulatory function. *rs2277311* has promoter, enhancer and DNase signatures  
 380 and the urate-decreasing A-allele disrupts a predicted HiC1 motif (Tables 3, S4) [35].

381

382 Six loci (*RREB1*, *INHBC*, *HLF*, *UBE2Q2*, *SFMBT1*, *HNF4G*) with PAINTOR causal  
 383 SNPs (PP > 0.8) also have colocalised eQTL (Tables 2 and 3). These loci represent  
 384 good candidates for follow up analyses of regulatory function (e.g. [11, 12]). The lead  
 385 urate variant at the *HLF* locus, *rs7224610* (PAINTOR posterior probability = 0.92) is  
 386 intronic, has enhancer signatures, is bound by multiple transcription factors including  
 387 POL2 (Table S4) and is amongst the maximally associated *trans*-eQTL variants for  
 388 *DMD* (encodes *dystrophin*). *rs675209* at *RREB1* is the maximal *trans*-eQTL variant for  
 389 *UTRN* (encodes *utrophin*), overlaps enhancer signatures in six tissues and alters 8  
 390 transcription factor binding motifs (Tables 3 and S4). The variants at *HNF4G*, *SFMBT1*,

391 *UBE2Q2* and *INHBC* do not overlap putative regulatory elements (Table S4). Although  
392 *rs13264750* (*HNF4G*), *rs2115779* (*SFBMT1*) and *rs9870898* (upstream of *SFMBT1*)  
393 are predicted to change 8 binding motifs including HNF1 (Table 3).

394

395 *SLC22A9*

396 *SLC22A9* encodes organic anion transporter 7 (OAT7). OAT7, expressed only in the  
397 liver, is a relatively poorly characterized member of the OAT family [36] that includes  
398 urate secretory transporters OAT1-3 and the urate reuptake transporter OAT4 (encoded  
399 by *SLC22A11*) [37]. RT-PCR screening of human cell lines indicated expression in  
400 HepG2 cells (Figure 4). OAT7 exhibited modest uricosuric-sensitive urate uptake when  
401 expressed in *Xenopus* oocytes (Figure 4). Pre-injection of oocytes with butyrate, but  
402 not other anions (data not shown), led to a modest trans-activation of urate transport,  
403 consistent with urate-butyrate exchange.

404

## 405 **Discussion**

406 *Identification of 15 new loci associated with serum urate*

407 The 15 new loci identified here as associated with serum urate levels can be ranked  
408 according to the strength of genetic evidence according to two criteria; a genome-wide  
409 significant association with serum urate levels, replication in gout, and/or replication in  
410 the recently published Japanese serum urate GWAS [6]. In addition to the strength of  
411 the genetic evidence, seven of these loci were co-localized with at least one eQTL signal  
412 which identifies a putative causal gene, and provides further evidence of a genuine  
413 association with serum urate levels. Of the 15 novel loci, eight (*FGF5*, *BICCI1*,  
414 *PLA2G16*, *B4GALT1*, *SLC22A9*, *AIP*, *FLRT1* and *USP2*) were genome-wide  
415 significant and replicated in gout (Table 1) or the Kanai *et al.* urate dataset [6]. The  
416 *HLA-DQB1* locus was genome-wide significant and a putative causal gene *HLA-DQA2*  
417 was identified. The *DHRS9*, *MLXIP*, *MRPS7*, *RAI14*, and *IDH2* loci were only of  
418 suggestive association in the trans-ancestral meta-analysis but the colocalization  
419 analysis provided strong evidence that they participate in a causal pathway. Of these  
420 five loci, we were able to replicate the association at *DHRS9*, *MLXIP*, *MRPS7*, *RAI14*  
421 and *IDH2* in gout, and for *MLXIP* we additionally replicated the association in the  
422 Kanai *et al.* [6] data. Overall, the evidence that these five loci, identified solely by  
423 colocalization of GWAS signal with an eQTL signal, have a true association with serum



424 urate is strong and provide empirical support for our genome-wide co-localization  
425 approach using sub-genome wide significant GWAS signals. Overall, we identified 14  
426 novel loci that we are confident are unlikely to represent false positive associations  
427 (*FGF5*, *B4GALT1*, *PLA2G16*, *SLC22A9*, *FLRT1*, *USP2*, *BICC1*, *DHRS9*, *RAI14*,  
428 *IDH2*, *MLXIP*, *AIP*, *MRPS7*, *HLA-DQB1*). The remaining locus *LINC00603* was  
429 identified only as genome-wide significant in the trans-ancestral meta-analysis.

430

431 A total of seven loci (three new, one independent signal, three previously reported) are  
432 concentrated in a 4 Mb segment of Chr 11 (63.2-67.2 Mb). In the previous Okada *et al.*  
433 and Kanai *et al.* East Asian and Japanese GWAS [5, 6] these loci were reported as a  
434 single locus. Köttgen *et al.* [4] reported three loci in this region (*SLC22A11*, *SLC22A12*  
435 and *OVOLI*). The Chr11 region is clearly of importance for serum urate control and  
436 there are more genome-wide associated loci in East Asian populations than in  
437 Europeans. At the *RELA* locus the causal variants in the East Asian population are not  
438 the same as in the European population (although we note that the Okada *et al.* [5] East  
439 Asian *RELA* signal is based entirely on imputed SNPs). Notably, the effect sizes of  
440 *SLC22A9* and *SLC22A12* (change in urate of 0.31 and 0.25 mg/dL per allele,  
441 respectively) are larger in East Asian populations than *SLC2A9* and *ABCG2* (0.18 and  
442 0.17 mg/dL, respectively). In comparison the effect sizes in Europeans for *SLC2A9*,  
443 *ABCG2* and *SLC22A12* are 0.21, 0.22 and 0.07 mg/dL, respectively (note that the lead  
444 *SLC22A9* SNP *rs11231463* is uncommon in Europeans (1.1%)). In Europeans  
445 *SLC22A12* is the seventh strongest signal in serum urate after *SLC2A9*, *ABCG2*, *GCKR*,  
446 *SLC17A1*, *SLC16A9* and *INHBC*.

447

448 Very recently a separate trans-ancestral meta-analysis of the Köttgen *et al.* [4] and a  
449 new serum urate GWAS of 121,745 Japanese individuals (that encompassed all the  
450 individuals in the Kanai *et al.* [6] study) was published [38]. This study, the largest  
451 serum urate GWAS published to date, discovered 59 loci, of which 22 are newly  
452 reported beyond those reported in the Köttgen *et al.* and Kanai *et al.* studies [4, 6]. Of  
453 the 22, three overlapped with the 15 newly identified loci in the study reported here  
454 (*HLA-DQB1*, *B4GALT1*, *USP2*). Both the Kanai *et al.* [6] and Nakatochi *et al.* [38]  
455 studies reported this segment of Chr11 as a single locus. Here we dissected the Chr11  
456 63.2-64.4 Mb segment and identified four loci in this region, including *SLC22A9*  
457 (encoding OAT7), the locus with the largest effect size on serum urate in the Japanese  
458 population (Table 1).

459

460 *Assigning causality to reported GWAS loci*

461 We identified 44 genes with strong evidence for colocalization with a serum urate  
462 association signal (24 from the *cis*-eQTL analysis and 20 from the *trans*-eQTL  
463 analysis). Candidate causal genes at seven loci deserve brief mention (in addition to  
464 those discussed in more detail later). First, *MUC1* encodes mucin-1 (CD227), a  
465 membrane protein with excessive O-glycosylation in the extracellular domain that  
466 protects from pathogens. Mutations in *MUC1* cause autosomal dominant  
467 tubulointerstitial kidney disease [39], suggesting that regulation of this gene could  
468 influence serum urate levels via an effect on the structure and function of the kidney  
469 tubule. Second, *IGF1R* encodes the insulin-like growth factor-1 receptor, with the  
470 eQTL implicating IGF-1 signalling and resultant anabolic processes in urate control.  
471 Third, *SLC16A9* encodes mono-carboxylate transporter 9 and the urate GWAS signal  
472 is also associated with DL-carnitine and propionyl-L-carnitine levels, which are both  
473 strongly associated with serum urate levels [40]. Kidneys reabsorb carnitine from the  
474 urinary filtrate by a sodium-dependent transport mechanism [41], possibly influencing  
475 urate levels indirectly as a result of the secondary sodium dependency of urate transport  
476 [37]. Fourth, *B4GALT1* encodes  $\beta$ -1,4-galactosyltransferase 1, a Golgi apparatus  
477 membrane-bound glycoprotein. This implicates sugar modification of proteins (e.g.  
478 urate transporters) in serum urate control, either by regulating their level of expression  
479 and / or activity. Fifth, *PRPSAP1* has a *cis*-eQTL at the *QRICH2* locus - *PRPSAP1*  
480 (encoding phosphoribosyl pyrophosphate synthetase-associated protein 1) is a strong  
481 candidate gene. As a negative regulator of phosphoribosyl pyrophosphate synthetase  
482 that catalyzes the formation of phosphoribosyl pyrophosphate from ATP and ribose-5-  
483 phosphate in the purine salvage pathway decreased expression of *PRPSAP1* would be  
484 predicted to contribute to increased urate levels. However, our data are not consistent  
485 with this hypothesis - *rs164009\_A* associated with increased *PRPSAP1* expression and  
486 increased urate levels. Sixth, a very strong colocalized *trans*-eQTL for *CHAC2* was  
487 identified at *INHBB*. *CHAC2* is a  $\gamma$ -glutamyl cyclotransferase involved in glutathione  
488 homeostasis [42, 43]. Proximal tubule cells contain high levels of glutathione which is  
489 transported in and out of the kidney via OAT1/3, MRP2/4 and OAT10 [44, 45].  
490 Specifically, glutathione serves as a counter ion for urate reabsorption via OAT10,  
491 releasing glutathione into the lumen [45]. Thus it could be predicted that changes in  
492 *CHAC2* expression would disrupt glutathione homeostasis altering urate  
493 secretion/reabsorption in the kidney. Finally, we note that there was no evidence for a

494 regulatory effect at *ABCG2* which is consistent with the strong evidence supporting  
495 p.Gln141Lys (*rs2231142*) as the dominant causal variant at that locus [13]. A similar  
496 scenario exists at *GCKR* where p.Leu446Pro (*rs1260326*) is the maximally-associated  
497 variant (Figure S5).

498

#### 499 *The dystrophin complex*

500 Of the 20 spatially supported *trans*-eQTL that colocalize with European GWAS serum  
501 urate signals, two genes, *DMD* and *UTRN* (*trans*-eQTL at *HLF* and *RREB*,  
502 respectively), also have serum urate association signals in *cis*. There was a sub-genome  
503 wide signal of association at the *UTRN* locus in the European serum urate GWAS data  
504 (*rs4896735*;  $P = 2.0 \times 10^{-04}$ ) [4] and a similar signal has been reported in an Indian  
505 serum urate GWAS study (*rs12206002*;  $P < 10^{-4}$ ; not in LD with *rs4896735*) [46].  
506 *DMD* associated with serum urate levels in the Japanese serum urate GWAS sample  
507 set (*rs1718043*;  $P = 8.8 \times 10^{-05}$ ) [6]. *UTRN* and *DMD* are components of the dystrophin  
508 complex and the urate-raising alleles at these *trans*-eQTL increase expression of *UTRN*  
509 and *DMD* (Table 2). The canonical function of the dystrophin complex is well defined  
510 from its role in Duchennes Muscular Dystrophy and is crucial for stabilisation of the  
511 plasma membrane in muscle cells [47]. However syntrophins within the dystrophin  
512 complex also act as scaffolding for transporters (e.g. *ABCA1* [48]) and ion channels  
513 via PDZ domains, reminiscent of the *PDZK1* interaction with urate transporters [37].  
514 Isoforms of the proteins within the dystropin complex have segment-specific  
515 distribution in the mouse nephron [49] thus it is possible that expression changes in the  
516 components of this complex in the kidney could alter the function of renal transporters  
517 that influence serum urate levels.

518

#### 519 *OAT7*

520 An East Asian-specific genome-wide significant signal near the gene encoding *OAT7*,  
521 *SLC22A9*, was confirmed. Ideally, we would have performed a colocalization analysis  
522 to assess whether this genetic association may be influencing the expression of  
523 *SLC22A9*. However, since *SLC22A9* is specifically expressed in the liver and brain and  
524 no East Asian eQTL are currently available for those tissues, this could not be  
525 performed. In lieu of providing genetic evidence that this association influences the  
526 expression of *SLC22A9*, we sought to evaluate whether *OAT7* transported urate. Our  
527 data suggest that *OAT7* is a very weak urate transporter in the presence of the various  
528 anions tested as exchangers (glutarate,  $\alpha$ -ketoglutarate, butyrate,  $\beta$ -hydroxybutyrate).

529 It is possible that OAT7 may function as a more efficient urate transporter in the  
530 presence of the appropriate (as yet unidentified) exchanging anion. OAT7 is a hepatic  
531 transport protein that exchanges, for the short chain fatty acid butyrate, sulphyl  
532 conjugates, xenobiotics and steroid hormones and is not inhibited by established  
533 inhibitors and substrates of other organic anion transporters such as probenecid,  
534 paraaminohippurate, nonsteroidal anti-inflammatory drugs and diuretics [36]. We  
535 found that urate transport mediated by OAT7 is inhibited by the uricosuric drugs  
536 benzbromarone and tranilast, which inhibit multiple other urate transporters [50]. Three  
537 uncommon missense variants that influence the ability of OAT7 to transport pravastatin  
538 by either causing the protein to be retained intracellularly or reducing protein levels at  
539 the plasma membrane have been reported [51], all at a frequency < 1% in East Asian.  
540 HNF4 $\alpha$  plays a key role in the transactivation of the *SLC22A9* promoter [51], an  
541 interesting observation given that HNF4 $\alpha$  is also required for expression of the gene  
542 encoding the urate transportosome-stabilizing molecule PDZK1 in the liver [11], and  
543 is implicated in control of serum urate levels via the *MAFTRR* locus [12].

544

#### 545 *Colocalization analysis assigns causation to variants at MLXIPL and MLXIP*

546 We identified the paralogs *MLXIPL* and *MLXIP* as the putative causal genes at the  
547 *BAZ1B* and *MLXIP* loci respectively. These genes encode the ChREBP and MondoA  
548 proteins, which are glucose-sensitive transcription factors involved in energy  
549 metabolism – including glycolytic targets and glycolysis [52-54]. These proteins form  
550 heterodimers with the Mlx protein, and both of these proteins are activated by high  
551 levels of intracellular glucose-6-phosphate – a product of the first step of the glycolysis  
552 and pentose phosphate pathways. Increased activity of the pentose phosphate pathway  
553 leads to the production of ribose-5-phosphate thus stimulating *de novo* purine  
554 nucleotide synthesis. The resulting nucleotides are ultimately catabolised into urate if  
555 they are not otherwise utilized. In *Drosophila* at least, the ChREBP/Mondo-Mlx  
556 complex is responsible for the majority of transcriptional changes that result from  
557 glucose consumption, including the pentose phosphate pathway [52]. The  
558 colocalization results reveal that the serum urate-increasing variants at both loci  
559 decrease expression of *MLXIPL* and *MLXIP*. Taken together, this suggests a possible  
560 mechanism whereby the decreased basal expression of ChREBP and MondoA results  
561 in increased activity of the pentose phosphate pathway and therefore higher levels of  
562 serum urate.

563

564 *MRPS7 and IDH2 and mitochondrial function*

565 *MRPS7* is putatively involved in serum urate control via mitochondrial processes. Of  
566 relevance, reduced relative mitochondrial DNA copy number is associated with gout  
567 [55]. The association signal at the *MRPS7* locus colocalized with gene expression of  
568 *MRPS7* and *GGA3*. *MRPS7* encodes the mitochondrial ribosomal protein S7, which is  
569 required for the assembly of the small ribosomal subunit of the mitochondria. A whole  
570 exome study revealed that a non-synonymous mutation in *MRPS7* (p.Met184Val),  
571 which destabilizes the protein and reduces expression, results in impaired  
572 mitochondrial protein synthesis and impaired mitochondrial function [56]. The patients  
573 in this study presented with congenital sensorineural and significant hepatic and renal  
574 impairment, consistent with a role for reduced *MRPS7* activity in renal function. Our  
575 findings show that the urate-increasing G-allele decreases the expression of *MRPS7*  
576 (Table 2), consistent with the hypothesis generated by the p.Met184Val phenotype.  
577 Also implicating mitochondrial function is *IDH2* which encodes isocitrate  
578 dehydrogenase that catalyzes the decarboxylation of isocitrate to 2-oxyglutarate in the  
579 citric acid cycle. The urate-increasing allele associates with reduced expression of  
580 *IDH2*. Somatic mutations in *IDH2* are implicated in a range of diseases including  
581 cancers such as glioma and acute myeloid leukemia (where an inhibitor is in phase III  
582 clinical trial [57]) and the tumor syndromes Ollier disease and Maffucci syndrome [58].  
583 Understanding the molecular mechanism of urate control by the *MRPS7* and *IDH2* loci  
584 locus could lead to insights into the mitochondrial processes that influence serum urate  
585 levels.

586

587 *Trans-ancestral functional fine-mapping identifies putative causal variants*

588 To connect GWAS loci where we identified candidate causal genes to an underlying  
589 causal variant, we performed trans-ancestral fine-mapping with PAINTOR using the  
590 kidney, gastrointestinal tract, and liver cell type group annotations as functional priors.  
591 We identified six loci (*RREB1*, *INHBC*, *HLF*, *UBE2Q2*, *SFMBT1*, *HNF4G*) that had  
592 colocalized eQTL and contained SNPs with high posterior probabilities of causality  
593 (>0.8). Two additional loci *SLC2A9* and *SLC22A12* also contained SNPs with high  
594 posterior probabilities of causality (>0.8) that were *cis* and *trans*-eQTL for *RP11-*  
595 *448G15.1* and *RNF169*, respectively. Many of these SNPs overlapped annotated  
596 regulatory regions of the genome (Table 3). These candidate causal variants and genes  
597 provide a starting point for understanding how these variants alter serum urate levels.  
598 The power of this approach is illustrated in our prior work on the *PDZK1* locus [11].

599 Here, we experimentally confirmed that *PDZK1* was the causal gene, with *rs1967017*  
600 (one of the two candidate causal variants identified with posterior probabilities >0.25  
601 (Table S1)) being a highly likely causal variant via altering a binding site for hepatocyte  
602 nuclear factor 4 $\alpha$ . We have also applied a similar approach to the *MAF* locus [12]. *MAF*  
603 is a complex locus with population-specific signals, and for one of these signals we  
604 experimentally demonstrated that the effect on urate arises from one of two SNPs  
605 within a kidney specific enhancer that is co-expressed with *MAF* and *HNF4A* in the  
606 developing proximal tubule. This study also identified colocalised eQTL for two long  
607 intergenic non-coding RNAs *MAFTRR* and *LINC01229* that regulate *MAF* expression  
608 in *cis*, and other genes implicated in urate metabolism in *trans* [12]. These studies  
609 highlight the power of initially combining colocalization analyses and fine-mapping  
610 using prior information to determine the molecular mechanisms that underlie GWAS  
611 signals.

612

613 In conclusion, we have identified 15 new GWAS signals associated with serum urate  
614 levels. By *cis*-eQTL colocalization we identified 24 candidate causal genes and by  
615 *trans*-eQTL analysis we implicated a further 20 genes in the molecular control of serum  
616 urate levels. Highlighted insights into molecular mechanisms come from identification  
617 of the protein encoded by *SLC22A9* (OAT7) to be a urate transporter, the implication  
618 of mitochondrial function via *MRPS7*, the identification of *MLXIP* (alongside the  
619 already identified *MLXIPL*) and intriguing data genetically implicating the dystrophin  
620 complex in control of serum urate levels.

621

## 622 **Methods**

### 623 *Data preparation and quality control*

624 Summary statistics from the Global Urate Genetics Consortium (GUGC) meta-analysis  
625 of GWAS data consisting of 110,238 individuals of European ancestry [4]  
626 (<http://metabolomics.helmholtz-muenchen.de/gugc/>), and a meta-analysis consisting of  
627 21,417 individuals of East Asian ancestry [5] were utilised. For both datasets the  
628 following quality control procedure was followed. Firstly, we removed any SNPs that  
629 were not present in the Phase 3 release of the 1000 Genomes for the representative  
630 populations (EUR and EAS), or where the alleles were not identical between this  
631 summary data and the 1000 Genomes (e.g. the alleles were G/T in the GUGC meta-



632 analysis and T/A in the 1000 Genomes dataset) [59]. The effective sample size for each  
633 SNP was calculated using the Genome-wide Complex Trait Analysis (GCTA, v1.25.2)  
634 toolkit [60] and SNPs with effective sample sizes  $> 2$  standard deviations from the mean  
635 were excluded. Finally, SNPs with a minor allele frequency (MAF) of less than 0.01  
636 were excluded.

637

#### 638 *Trans-ancestral meta-analysis*

639 ImpG (v1.0) was used to impute Z-scores into the European and East Asian summary  
640 statistics. For the reference haplotypes the Phase 3 release of the 1000 Genomes project  
641 was used [59], and only bi-allelic SNP markers having a minor allele frequency greater  
642 than 0.01 in the relevant population were included. All imputed markers with a  
643 predicted  $R^2$  of less than 0.8 were removed. Meta-analysis was performed by summing  
644 the Z-scores and weighting by sample size. For the imputed SNPs, the sample size was  
645 estimated as the median of the sample size of the SNPs where this information was  
646 available. To provide an adjustment for inflated test statistics, the LD-score intercept in  
647 the original summary statistics files was calculated using LD-score regression [61].  
648 This intercept adjusts the test statistics for confounding, such as cryptic relatedness, but  
649 in contrast to genomic control will not remove inflation caused by a true polygenic  
650 signal.

651 Independent regions were identified using the following protocol. Firstly, SNPs that  
652 were genome-wide significant ( $P < 5 \times 10^{-08}$ ) were padded 50 kb either side of the SNP  
653 position, and all overlapping regions were clumped together. Secondly, the maximal  $R^2$   
654  $> 0.6$  for the most significant SNP in each of these regions was calculated for each  
655 population. Finally, the maximal regions from the P-value clumping and LD approach  
656 were created, and any overlapping regions were merged. SNPs that were not present in  
657 both datasets were also analyzed, and for those SNPs the LD was only calculated in the  
658 relevant population. Based on their proximity to stronger signals four loci  
659 (*Chr4/rs114188639/CLNK1*, *Chr8/rs2927238/HNF4G*, *Chr11/rs641811/FLRT1*,  
660 *Chr11/rs117595559/VPS51*) were visually examined by LocusZoom and subjected to  
661 conditional analysis – of these only *rs641811/FLRT1* was concluded to be independent  
662 of the nearby signal. For all significant SNPs, the meta-analysis effect estimate was  
663 calculated using the inverse variance method, and when there was no effect estimate, it  
664 was estimated from the Z score using the following equation (1).

665

666 *Equation 1*

$$\hat{\beta}_x = Z_x S_x$$
$$S_x = 1/\sqrt{2p(1-p)(\hat{n} + z_x^2)}$$
$$\hat{n} = \text{median}(n)$$

667

668 *Conditional analysis*

669 A conditional and joint analysis of the European summary statistics for all genome-  
670 wide significant regions identified by meta-analysis was done. This was not done on  
671 the East Asian summary statistics owing to the lack of availability of both a LD matrix  
672 and a reference haplotype set of sufficient size. For all imputed SNPs the effect estimate  
673 was calculated as above (equation 1). The genotypic data from the UK Biobank was  
674 used as the reference for the LD, and to improve computational efficiency only a  
675 random 15% (22,872) of samples were included. Since the GCTA-COJO module [62]  
676 was not designed to utilize dosage matrices, we performed this analysis using our own  
677 software, Correlation-based Conditional analysis (COCO:  
678 <https://github.com/theboocock/coco>) which, based on the methods presented in GCTA-  
679 COJO [62], was designed to perform conditional and joint analysis from summary  
680 statistics with some minor alterations to use LD correlation matrices as input. To  
681 discover conditional associations, the coco pipeline implemented a forward stepwise  
682 selection using a residual-based regression. First, SNPs were ranked on marginal test  
683 statistics, then the top SNP was selected and the result of extracting the residuals from  
684 this model and performing a regression with every other SNP was estimated. These  
685 test-statistics were then ranked. If the new top SNP passed the P-value threshold it was  
686 added to a joint model with the other selected SNP, which was used as the new model  
687 for residual extraction. This process was then repeated until no SNPs passed the  
688 significance threshold. In practice, we restricted the maximum number of selected  
689 SNPs at a locus to five (there is evidence for multiple signals at *SLC24A9* [10]), and we  
690 did not consider any pairs of SNPs having an  $R^2 > 0.9$ . To ensure that the method was  
691 working correctly, simple phenotypes were simulated and it was verified that COCO  
692 yields almost identical results to the lm function in the R programming language.

693

694 A mathematical explanation of the method is given as follows. We assume we have  
695 mean centered genotypes in a matrix X. To perform GWAS we generate a marginal  
696 statistic for each variant individually (Equation 2).

697



698 *Equation 2*

$$699 \quad \hat{\beta}_{gwas} = (diag(X'X))^{-1}x'y$$

700

701 Using substitution into the ordinary least squares equations we can convert these  
702 marginal effects into joint effects, and also calculate the standard error (Equation 3).

703

704 *Equation 3*

$$\begin{aligned} \hat{\beta}_{joint} &= (X'X)^{-1}diag(X'X)\hat{\beta}_{gwas} \\ var(\hat{\beta}) &= \sigma_j^2(X'X)^{-1} \\ \hat{\sigma}_j^2 &= \frac{y'y - \hat{\beta}_{joint}diag(X'X)\hat{\beta}_{gwas}}{n - N - 1} \end{aligned}$$

705

706

707 Where N is equal to the number of SNPs in the joint model. Finally, we can approximate  
708 a regression of the residuals from a joint model (Equation 4).

709

710 *Equation 4*

$$\begin{aligned} \hat{\beta}_{resid1} &= \hat{\beta}_{gwas1} - (X'_1X_1)^{-1}(X'_1X_2)(X'_2X_2)^{-1}diag(X'_2X_2)\hat{\beta}_{gwas2} \\ var(\hat{\beta}_{resid1}) &= \frac{(y'y - \hat{\beta}'_{joint2}diag(X'_2X_2)\hat{\beta}_{gwas2} - \hat{\beta}_{resid1}diag(X'_1X_1)\hat{\beta}_{resid1})(X'_1X_1)^{-1}}{n - N - 1} \end{aligned}$$

711

712

713 Where X<sub>1</sub> is the genotype matrix of SNPs to be regressed on by the residuals, X<sub>2</sub> is the  
714 genotype matrix of the joint model, and N is equal to the number of SNPs in the residual  
715 model. In practice the data matrix X is unavailable as summary statistics were used, but  
716 it is possible to approximate this matrix using the LD structure from a reference panel  
717 (Equation 5).

718

719 *Equation 5*

$$\begin{aligned} diag(R'R)_{11} &= (n - 1)var(R_1) \\ X'X &\approx diag(R'R)cor(R'R)diag(R'R) \end{aligned}$$

720

721

722 Where R is the reference genotype matrix, sigma is the LD matrix for the locus, and  
723 the diagonal of R'R is modified to be equal to the sample size of the SNP minus one in

724 the GWAS multiplied by the genotypic variance of the SNP observed in the reference  
725 panel. Since the data were generated from dosages and not hard-called genotypes, using  
726 the observed genotypic variance in the reference panel would have accounted for some  
727 of the uncertainty introduced by imputation.

728

729 To calculate the effective number of hypothesis tests, Eigen value decomposition was  
730 performed on the SNP correlation matrix for each region, using data from the European  
731 individuals from the 1000 Genomes Project. The number of hypotheses tested per  
732 region was calculated as the number of Eigen values that were required to explain 0.995  
733 of the total sum of the Eigen values. The total number of hypotheses tested in the  
734 conditional analysis was taken as the sum of the per region hypothesis counts [63]. This  
735 revealed that in the focused conditional analysis, we were performing approximately  
736 5,443 hypothesis tests. The multiple-testing threshold for our conditional analysis was  
737 therefore determined to be  $9.2 \times 10^{-6}$  ( $0.05/5443$ ).

738

739

740 *Equation 6*

$$\frac{\sum_{m=1}^{M_{gao}} \lambda_m}{\sum_{m=1}^M \lambda_m} \geq c$$

741

742

743 The following equation was used to calculate variance explained by each SNP in the  
744 meta-analysis and joint analysis (Equation 7).

745

746

*Equation 7*

$$q^2 = \frac{Var(X)\beta^2}{Var(Y)}$$

747

748

749 Where  $Var(X)$  was the variance for each SNP, calculated as  $2p(1 - p)$  with  $p$  as the  
750 allele frequency.  $\beta$  was the effect estimate, and  $Var(Y)$  was calculated as the pooled  
751 variance estimate provided by the GCTA software when performing the conditional  
752 analysis. This pooled variance was calculated using the equation below (Equation 8).

753

$$s_p^2 = \frac{\sum_{i=1}^k (n_i - 1) s_i^2}{\sum_{i=1}^k (n_i - 1)}$$

754

755 Where  $s_i^2$  was the phenotypic variance estimated by the GCTA software for each  
756 chromosome, and  $n_i$  was the number of SNPs on each chromosome. This revealed that  
757 the empirical variance of sex adjusted serum urate was 1.624. Unadjusted variance in  
758 serum urate was also calculated using the equation above, where  $s_i^2$  was replaced with  
759 the variance in serum urate for each study, and  $n_i$  was replaced with the number of  
760 participants in each study. This analysis revealed that the empirical variance of  
761 unadjusted serum urate was 1.964.

762

### 763 *Heritability and functional enrichments*

764 LD Score regression was used to partition SNP heritability of serum urate [61]. An  
765 estimate was generated using LD Score for the amount of heritability explained by all  
766 SNPs additively in the Köttgen *et al.* [4] meta-analysis. We also performed functional  
767 annotation-partitioned LD score regression to determine which cell type groups and cell  
768 types contribute significantly to the heritability of serum urate [64]. The comprehensive  
769 set of functional annotations that were released with partitioned LD Score regression  
770 (<https://data.broadinstitute.org/alkesgroup/LDSCORE/>) were used. This works by  
771 comparing the results to a baseline model that contains annotations such as evolutionary  
772 conservation, and pooled cell type annotations such as DNaseI hypersensitivity. We  
773 calculated P-values and Bonferonni-corrected thresholds by dividing by the total  
774 number of tests within each of the cell type group and cell type specific analyses, noting  
775 that this is a conservative adjustment because the annotations are correlated. Benjamini-  
776 Hochberg false discovery rate (FDR) adjusted P-values were also calculated [65]. All  
777 results were visualized using ggplot2 [66].

778

### 779 *Functional trans-ancestral fine mapping with PAINTOR*

780 PAINTOR (v3.0) [67] was initially used to fine map the 38 loci associated at a genome-  
781 wide level of significance in this study with serum urate within the separate European  
782 and East Asian GWAS. This initial analysis revealed that both the *RELA* and *HLA* loci  
783 were inappropriate loci for trans-ancestral fine-mapping. For the *RELA* locus, the  
784 association signal between the European and East Asian GWAS clearly involves

785 different causal variants. For *HLA-DQBI*, the large number of SNPs in the region  
786 resulted in computational errors in the PAINTOR software. Both of the loci were  
787 excluded from all additional PAINTOR analyses. Cell type groups that were significant  
788 in the LD score regression analysis were used with PAINTOR. To assess how much  
789 the East Asian GWAS and these functional annotations improved serum urate fine-  
790 mapping, the average size of the 90% causal credible sets in three analyses was  
791 calculated.

- 792 1. European GWAS.
- 793 2. European and East Asian GWAS.
- 794 3. European and East Asian GWAS and functional annotations.

795

#### 796 *Cis-eQTL identification*

797 We used COLOC [68] to colocalize the urate-associated loci with publicly available  
798 eQTL data from the Genotype Tissue Expression Project (GTEx v6p). COLOC is a  
799 Bayesian method that compares four different statistical models at a locus. These  
800 models are: no causal variant in the GWAS or the eQTL region; a causal variant in  
801 either the GWAS or the eQTL region, but not both; different causal variants in the  
802 GWAS and the eQTL region; or a shared causal variant in the GWAS and the eQTL  
803 region. All the *cis*-eQTL regions from a GTEx tissue were merged with the genome-  
804 wide European serum urate GWAS data. Genes that were annotated as novel transcripts  
805 were removed. For learning the priors each *cis*-eQTL region was treated as independent  
806 and the likelihood was maximized using the Nelder-mead algorithm. Genes that had a  
807 posterior probability of colocalization greater than 0.8 were considered to have a shared  
808 causal variant with serum urate. We did not restrict our analysis only to the genome-  
809 wide significant loci, which made it possible to identify novel serum urate loci. If  
810 multiple tissues supported colocalization at probability  $> 0.8$  the posterior probability  
811 was averaged.

812

#### 813 *Trans-eQTL identification*

814 The Contextualize Developmental SNPs using 3D Information (CoDeS3D) algorithm  
815 (GitHub, <https://github.com/alcamerone/codes3d>) [69] was used to identify long-  
816 distance regulatory relationships for serum urate-associated SNPs. This analysis  
817 leverages known spatial associations from Hi-C databases [70] and gene expression  
818 associations (eQTL data from the GTEx catalogue [71]) to assess regulatory  
819 connections. Briefly, SNPs were mapped onto Hi-C restriction fragments, the genes

820 that physically interact with these restriction fragments identified and collated (SNP-  
821 gene spatial pairs). SNP-gene pairs were screened through GTEx to identify eQTL. The  
822 FDR was calculated using a stepwise Benjamini-Hochberg correction procedure and  
823 incorporated the number of tests and eQTL value list. An FDR value of  $< 0.05$  was  
824 accepted as statistically significant [69]. COLOC was then used to co-localize *trans*-  
825 eQTL with serum urate GWAS signals.

826

### 827 *Gout case-control sample sets for replicating serum urate associations*

828 The Japanese gout data set, generated as previously described, [30] consisted of 945  
829 male gout patients and 1,213 male controls, where gout was clinically ascertained. The  
830 Chinese data set, generated as previously described [32], consisted of 1,255 male gout  
831 cases and 1,848 male control where gout was clinically ascertained according to the  
832 American College of Rheumatology diagnostic criteria. The European gout dataset was  
833 generated from 7,342 gout patients and 352,534 controls of European ancestry from the  
834 UK Biobank [31], where gout was ascertained by self-report of physician-diagnosed  
835 gout or use of urate-lowering therapy [72]. Gout association in UK Biobank was tested  
836 using logistic regression, adjusted by age, sex, and the first 10 principal components  
837 (out of 40).

838

### 839 *SLC22A9 – Cell lines, RNA Extraction and RT-PCR*

840 Human kidney proximal tubule epithelial cell line (PTC-05) was obtained from Ulrich  
841 Hopfer (Case Western Reserve University, Cleveland, Ohio) and grown ( $37^{\circ}\text{C}$  in a 5%  
842  $\text{CO}_2$ ) on type IV collagen-coated Petri dish in a 1:1 mixture of DMEM and HAM'S  
843 F12 media containing 5 mM glucose, 10% fetal bovine serum (FBS), 2 mM glutamine,  
844 1 mM pyruvate, 5  $\mu\text{g}/\text{ml}$  transferrin, 5  $\mu\text{g}/\text{ml}$  insulin, 10 ng/ml human epidermal growth  
845 factor, 4  $\mu\text{g}/\text{ml}$  dexamethasone, 15 mM HEPES (pH 7.4), 0.06%  $\text{NaHCO}_3$ , 10 ng/ml  
846 interferon-gamma, 50  $\mu\text{M}$  ascorbic acid, 20 nM sodium selenite ( $\text{Na}_2\text{SeO}_3$ ), 1nM  
847 triiodothyronin (T3) and penicillin (50 units/ml) / streptomycin (50  $\mu\text{g}/\text{ml}$ ). Human  
848 embryonic kidney HEK293 cells (ATCC) and human hepatocellular carcinoma HEPG2  
849 cells (ATCC) were grown ( $37^{\circ}\text{C}$  in a 5%  $\text{CO}_2$ ) and maintained in Dulbecco's Modified  
850 Eagle's Medium (DMEM) and Eagle's Minimum Essential Media (EMEM),  
851 respectively, supplemented with 4.5 g/L glucose, 2 mM glutamine, 1 mM sodium  
852 pyruvate, 10% FBS and penicillin (50 units/ml)/streptomycin (50  $\mu\text{g}/\text{ml}$ ).

853

854 Total RNA from human cell lines (PTC-05, HepG2 and HEK-293T) was extracted  
855 using spin columns with the RNeasy Mini Kit (QIAGEN, GmbH, Germany) following  
856 the manufacturer's instructions. Approximately 2 µg of DNase-treated total RNA,  
857 isolated from cells, was primed with poly-dT and random hexamers and then reverse-  
858 transcribed using AMV reverse transcriptase (New England Biolabs, Ipswich, MA). An  
859 equal amount of cDNA was used for PCR amplification of OAT7 and GAPDH cDNAs  
860 using the following primers, followed by electrophoresis.

861 hOAT7-2S [sense] 5'-CAACCTCAATGGCCTTTCAGGACCTCCTGG-3'

862 hOAT7-3A [antisense] 5'-GCCTGGAATCTGTGTGTTGCCCACTCGG-3'

863 hGAPDH-1S [sense] 5'-CGGAGTCAACGGATTTGGTTCGTATTG-3'

864 hGAPDH-1A [antisense] 5'-GACTGTGGTCATGAGTCCTTCCACGA-3'

865

866 *SLC22A9 - urate transport analysis of OAT7*

867 Studies using *Xenopus laevis* oocytes were performed in accordance with the Guide for  
868 the Care and Use of Laboratory Animals as adopted and promulgated by the U.S.  
869 National Institutes of Health, and were approved by the Institution's Animal Care and  
870 Use Committee. Mature female *Xenopus laevis* frogs (NASCO, Fort Atkinson, MI)  
871 were subjected to partial ovariectomy under tricane (SIGMA St Louis, MO) anesthesia  
872 (0.17% for 15–20 min) as described previously [50]. A small incision was made in the  
873 abdomen and a lobe of ovary was removed. Subsequently, the oocytes were pre-washed  
874 for 20 min in Ca<sup>2+</sup>-free ND96 medium (96 mM NaCl, 2 mM KCl, 1 mM MgCl<sub>2</sub>, 5 mM  
875 HEPES, pH 7.4) to remove blood and damaged tissue. Oocytes were then defolliculated  
876 by treatment with 3.5 mg/ml of collagenase enzyme (Roche, Indianapolis, IN) in Ca<sup>2+</sup>-  
877 free ND96 medium for about 120 min with gentle agitation at room temperature (25°C).  
878 Subsequent to this treatment, oocytes were washed three times with ND96 medium,  
879 and incubated (16-18 °C) in isotonic Ca<sup>2+</sup>-containing ND96 medium (96 mM NaCl, 2.0  
880 mM KCl, 1.8 mM CaCl<sub>2</sub>, 1.0 mM MgCl<sub>2</sub> and 5 mM Hepes, pH 7.4) supplemented with  
881 2.5 mM pyruvate and gentamycin (10 µg/ml).

882

883 For expression of OAT7 and OAT1 in *Xenopus laevis* oocytes, their respective full-  
884 length cDNAs were cloned into the pGEMHE vector, wherein the cDNA insert is  
885 flanked by the *Xenopus laevis* β-globin 5'-UTR and 3'-UTR [73]. These constructs were  
886 linearized and cRNAs were synthesized *in vitro* using T7 RNA polymerase  
887 (mMESSAGE mMACHINE; Ambion, Austin, TX) following the supplier's protocol.  
888 Isopropanol-precipitated, *in vitro* transcribed capped cRNAs were washed twice with

889 70% ethanol, the cRNA pellet was dried and then dissolved in sterile nuclease-free  
890 water. The yield and integrity of the capped cRNA samples was assessed by  
891 spectroscopy (at 260 nm) and 1% agarose-formaldehyde gel electrophoresis  
892 respectively. All cRNA samples were stored frozen in aliquots at -80 °C until used.

893

894 About 18 hours after isolation, oocytes were microinjected with 50 nl of sterile water,  
895 50 mM tris pH 7.4, or 50 nl of a cRNA solution in 50 mM tris buffer (pH 7.4) containing  
896 25 ng of the indicated cRNA using fine-tipped micropipettes by a microinjector (World  
897 Precision Instrument Inc. Sarasota, FL). The microinjected oocytes were then incubated  
898 in isotonic ND96 medium (pH 7.4) containing 1.8 mM CaCl<sub>2</sub>, 2.5 mM pyruvate,  
899 gentamycin (10µg/ml) at 16-18 °C for approximately 48 h to allow expression of  
900 protein from microinjected cRNA.

901

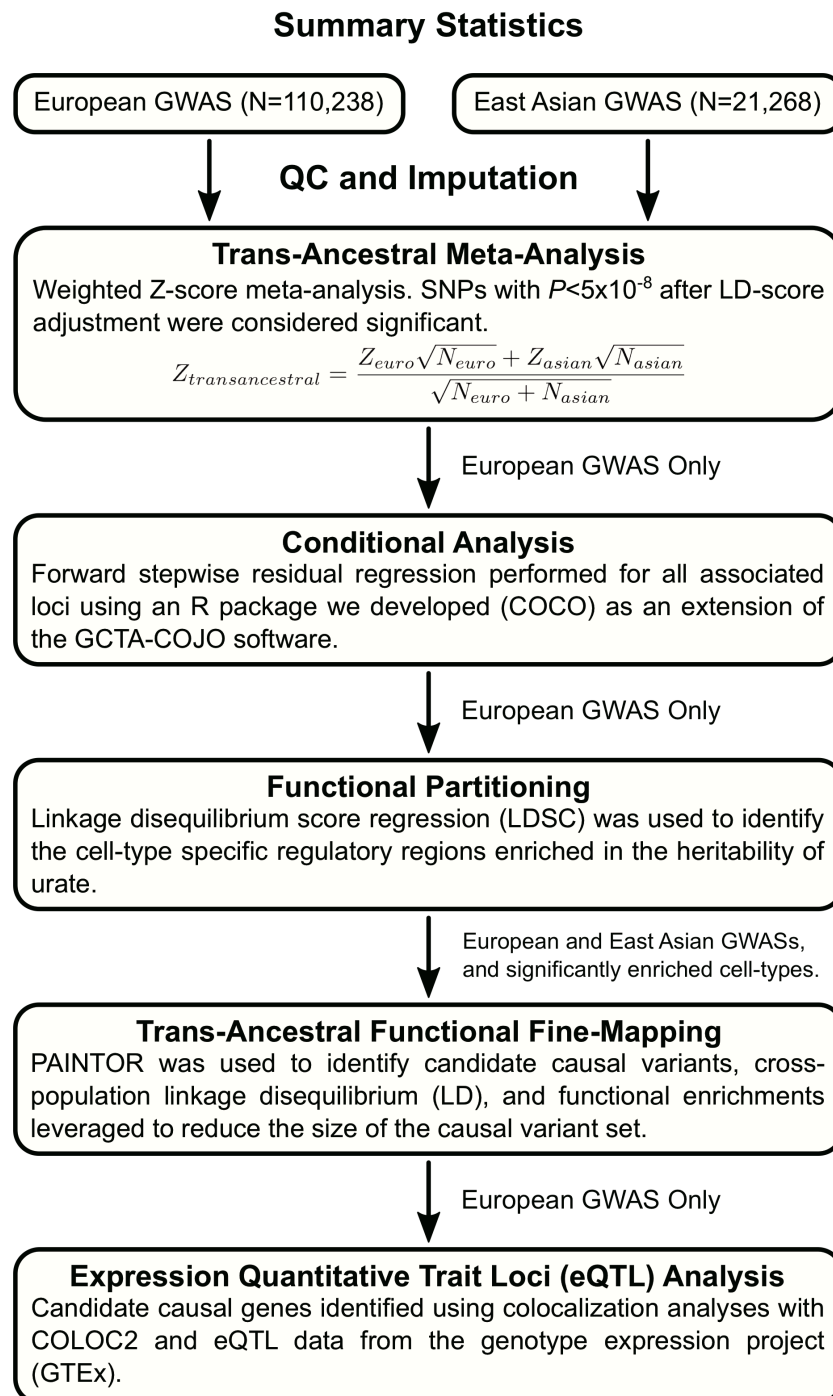
902 For [<sup>14</sup>C]-urate (specific activity: 50 mCi/mmol) uptake experiments in *Xenopus laevis*  
903 oocytes, oocytes expressing proteins as indicated (OAT7 and OAT1) were washed four  
904 times with ND96 medium (96 mM NaCl, 2.0 mM KCl, 1.8 mM CaCl<sub>2</sub>, 1.0 mM MgCl<sub>2</sub>  
905 and 5 mM Hepes, pH 7.4) without pyruvate and gentamycin. OAT7 functions as a  
906 butyrate exchanger [36], therefore OAT7-expressing oocytes were microinjected with  
907 50 nl of 100 mM butyrate to optimize urate transport by “trans-activation” [50]. After  
908 approximately 60 min of starvation, oocytes were preincubated in the ND96 uptake  
909 medium for 30 min before incubation (25°C, in a horizontal shaker-incubator) in the  
910 uptake medium containing [<sup>14</sup>C]-urate (40 µM). After 60 min of incubation in the  
911 uptake medium, oocytes (20 per group) were washed three times with ice-cold uptake  
912 medium to remove external adhering radioisotope. OAT7-expressing oocytes were then  
913 exposed to DMSO (diluent for uricosurics) or the uricosuric drugs tranilast and  
914 benzbromarone, as indicated. The radioisotope content of each individual oocyte was  
915 measured by scintillation counter following solubilization in 0.3 ml of 10% (v/v) SDS  
916 and addition of 2.5 ml of scintillation fluid (Ecoscint). All uptake experiments included  
917 at least 20 oocytes in each experimental group; statistical significance was defined as  
918 two-tailed  $P < 0.05$ , and results were reported as means ± S. E. Statistical analyses  
919 including linear regressions and significance were determined by Student's t test using  
920 SigmaPlot software.

921

922



Figure 1



923

924 **Figure 1. Analysis flowchart.**

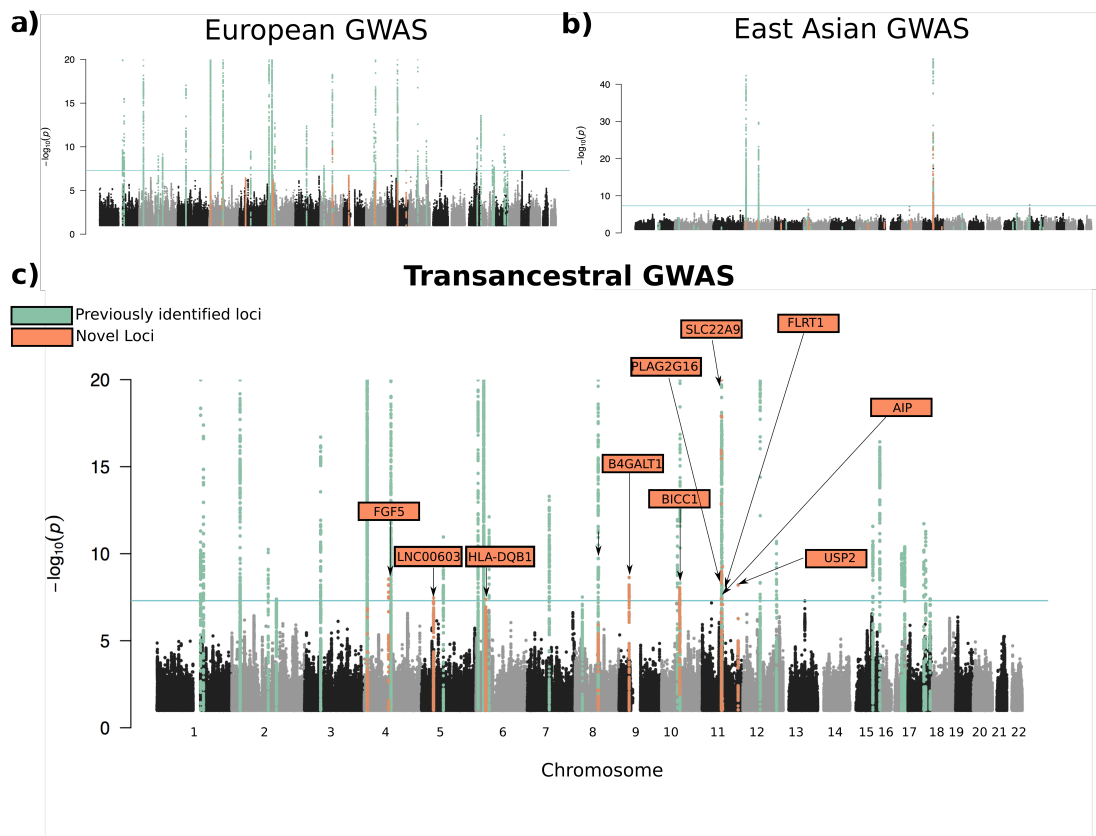
925

926

927

928

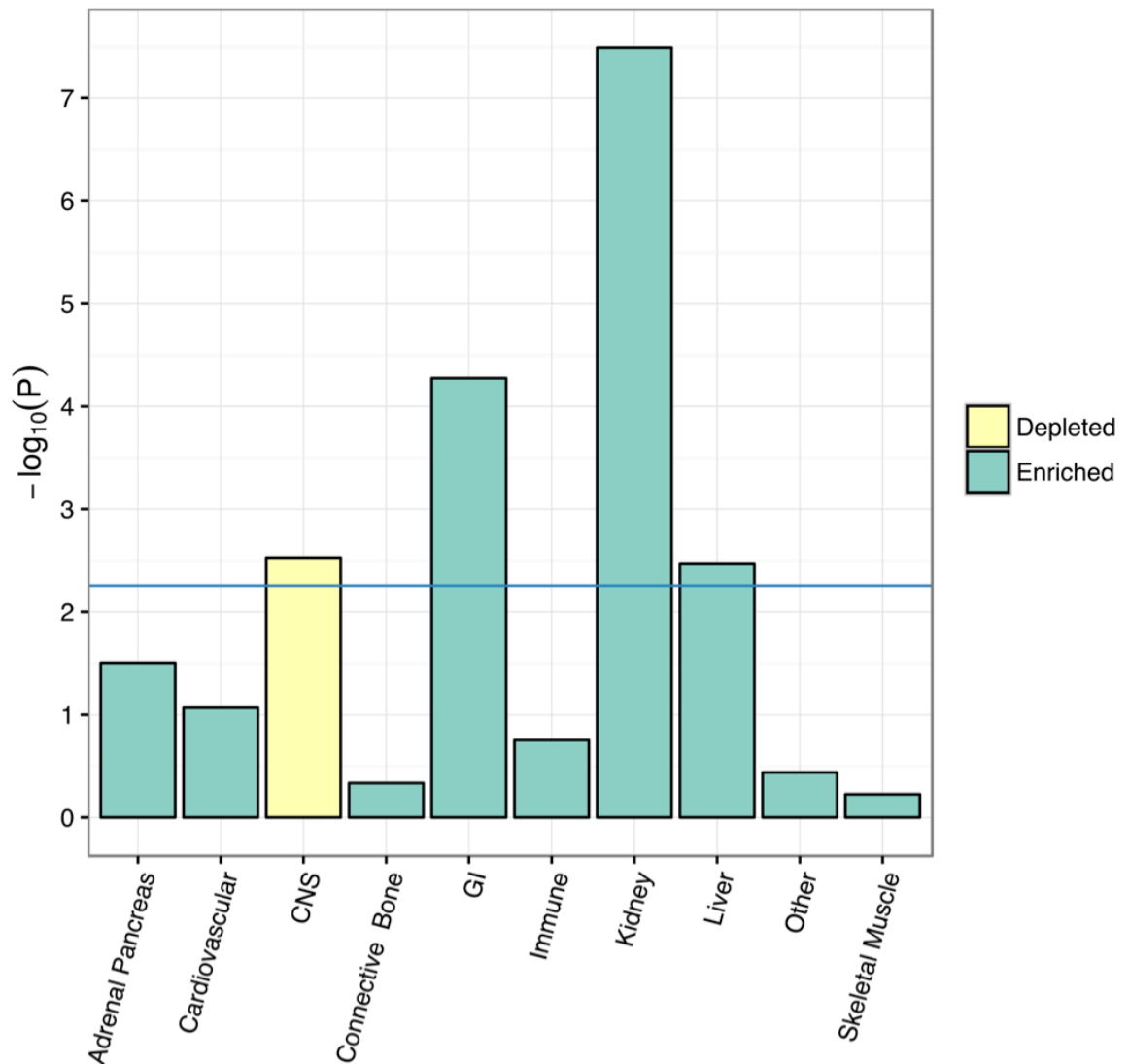




929

930 **Figure 2. Manhattan plots showing  $-\log_{10}(P)$  for all SNPs of the European, East**  
931 **Asian, and trans-ancestral GWAS ordered by chromosomal position. (A)**  
932 **Manhattan plot of the European GWAS. (B) Manhattan plot of the East Asian GWAS.**  
933 **(C) Manhattan plot of the trans-ancestral GWAS. SNPs within previously identified**  
934 **serum urate loci are colored light green. SNPs located within novel serum urate loci are**  
935 **colored orange. For the ten new genome-wide significant loci identified by trans-**  
936 **ancestral meta-analysis, the closest gene to the lead SNP is indicated.**

Figure 3.



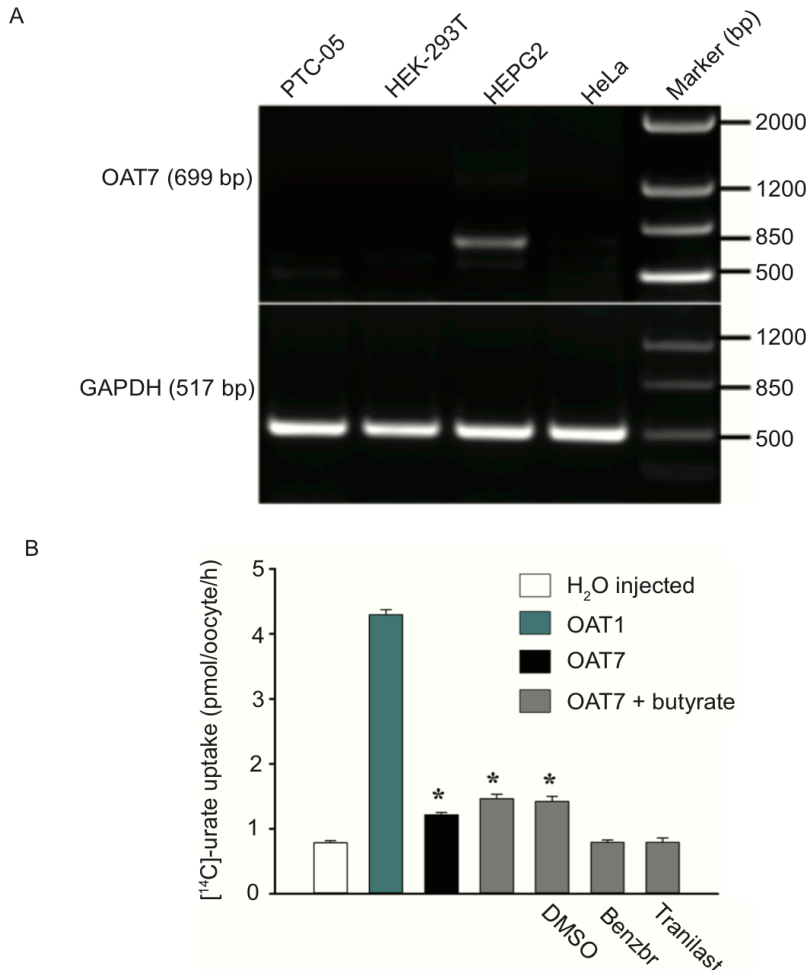
937

938 **Figure 3. Tissue-focused functional heritability enrichments.**

939 Tissue-focused functional heritability enrichments for serum urate levels. The color of  
940 each bar indicates whether heritability was depleted or enriched within a particular cell-  
941 type group. The  $-\log_{10}$  P-value for the enrichment in each cell-type group is on the Y-  
942 axis. These enrichments were generated using LD-Score functional partitioning of the  
943 European GWAS summary statistics.

944

Figure 4.



945

946 **Figure 4. Expression analysis and functional expression of *SLC22A9* (OAT7).**

947 (A) RT-PCR of *SLC22A9*/OAT7 expression in the human PTC-05 proximal tubular  
948 cell line, HEK-293T cells, and HepG2 hepatic cells. All three cell lines are positive for  
949 GAPDH but *SLC22A9*/OAT7 is unique to HepG2. (B) OAT7 is a weak urate  
950 transporter. *Xenopus* oocytes were microinjected with water (control cells) or cRNA  
951 for OAT1 or OAT7. OAT7-expressing cells have a very modest urate transport activity  
952 that is increased by prior microinjection with butyrate, to “trans-activate” urate-butyr-  
953 ate exchange. This transport activity is inhibited by the uricosurics tranilast and  
954 benzbromarone, each at a concentration of 100  $\mu$ M; DMSO, the diluent for tranilast  
955 and benzbromarone, has no effect on urate transport. \* refers to  $P < 0.001$  compared to  
956 OAT7-expressing cells without butyrate pre-injection and water control cells. Data  
957 shown are from a single representative experiment.

## 958 **Acknowledgements**

959 This research has been conducted using the UK Biobank Resource under Application  
960 Number 12611. Akiyoshi Nakayama is thanked for statistical analytic support. The  
961 Health Research Council of New Zealand is acknowledged for funding support.

## 962 **References**

- 963 1. Kuo CF, Grainge MJ, Zhang W, Doherty M. Global epidemiology of gout:  
964 prevalence, incidence and risk factors. *Nat Rev Rheumatol*. 2015;11(11):649-62.
- 965 2. Dalbeth N, Merriman TR, Stamp LK. Gout. *The Lancet*.  
966 2016;388(10055):2039-52.
- 967 3. Martinon F, Petrilli V, Mayor A, Tardivel A, Tschopp J. Gout-associated uric  
968 acid crystals activate the NALP3 inflammasome. *Nature*. 2006;440(7081):237-41.
- 969 4. Kottgen A, Albrecht E, Teumer A, Vitart V, Krumsiek J, Hundertmark C, et al.  
970 Genome-wide association analyses identify 18 new loci associated with serum urate  
971 concentrations. *Nat Genet*. 2013;45(2):145-54.
- 972 5. Okada Y, Sim X, Go MJ, Wu JY, Gu D, Takeuchi F, *et al*. Meta-analysis  
973 identifies multiple loci associated with kidney function-related traits in east Asian  
974 populations. *Nat Genet*. 2012;44(8):904-9.
- 975 6. Kanai M, Akiyama M, Takahashi A, Matoba N, Momozawa Y, Ikeda M, *et al*.  
976 Genetic analysis of quantitative traits in the Japanese population links cell types to  
977 complex human diseases. *Nat Genet*. 2018;50(3):390-400.
- 978 7. Phipps-Green AJ, Merriman ME, Topless R, Altaf S, Montgomery GW,  
979 Franklin C, *et al*. Twenty-eight loci that influence serum urate levels: analysis of  
980 association with gout. *Ann Rheum Dis*. 2016;75(1):124-30.
- 981 8. Urano W, Taniguchi A, Inoue E, Sekita C, Ichikawa N, Koseki Y, *et al*. Effect  
982 of genetic polymorphisms on development of gout. *J Rheumatol*. 2013;40(8):1374-8.
- 983 9. Major TJ, Dalbeth N, Stahl EA, Merriman TR. An update on the genetics of  
984 hyperuricaemia and gout. *Nat Rev Rheumatol*. 2018;14(6):341-53.

- 985 10. Merriman TR. An update on the genetic architecture of hyperuricemia and gout.  
986 *Arthritis Res Ther.* 2015;17(1):98.
- 987 11. Ketharnathan S, Leask M, Boocock J, Phipps-Green AJ, Antony J, O'Sullivan  
988 JM, *et al.* A non-coding genetic variant maximally associated with serum urate levels  
989 is functionally linked to HNF4A-dependent PDZK1 expression. *Hum Mol Genet.*  
990 2018;27(22):3964-73.
- 991 12. Leask M, Dowdle A, Salvesen H, Topless R, Fadason T, Wei W, *et al.*  
992 Functional Urate-Associated Genetic Variants Influence Expression of lincRNAs  
993 LINC01229 and MAFTRR. *Front Genet.* 2018; DOI: 10.3389/fgene.2018.00733.
- 994 13. Cleophas MC, Joosten LA, Stamp LK, Dalbeth N, Woodward OM, Merriman  
995 TR. ABCG2 polymorphisms in gout: insights into disease susceptibility and treatment  
996 approaches. *Pharmgenomics Pers Med.* 2017;10:129-42.
- 997 14. Ichida K, Matsuo H, Takada T, Nakayama A, Murakami K, Shimizu T, *et al.*  
998 Decreased extra-renal urate excretion is a common cause of hyperuricemia. *Nat*  
999 *Commun.* 2012;3:764.
- 1000 15. Matsuo H, Takada T, Ichida K, Nakamura T, Nakayama A, Ikebuchi Y, *et al.*  
1001 Common defects of ABCG2, a high-capacity urate exporter, cause gout: a function-  
1002 based genetic analysis in a Japanese population. *Sci Transl Med.* 2009;1(5):5ra11.
- 1003 16. Nakayama A, Matsuo H, Nakaoka H, Nakamura T, Nakashima H, Takada Y, *et*  
1004 *al.* Common dysfunctional variants of ABCG2 have stronger impact on hyperuricemia  
1005 progression than typical environmental risk factors. *Sci Rep.* 2014;4:5227.
- 1006 17. Woodward OM, Tukaye DN, Cui J, Greenwell P, Constantoulakis LM, Parker  
1007 BS, *et al.* Gout-causing Q141K mutation in ABCG2 leads to instability of the  
1008 nucleotide-binding domain and can be corrected with small molecules. *Proc Natl Acad*  
1009 *Sci U S A.* 2013;110(13):5223-8.
- 1010 18. Morris AP. Transethnic meta-analysis of genomewide association studies.  
1011 *Genet Epidemiol.* 2011;35(8):809-22.

- 1012 19. Zaitlen N, Pasaniuc B, Gur T, Ziv E, Halperin E. Leveraging genetic variability  
1013 across populations for the identification of causal variants. *Am J Hum Genet.*  
1014 2010;86(1):23-33.
- 1015 20. Consortium EP. An integrated encyclopedia of DNA elements in the human  
1016 genome. *Nature.* 2012;489(7414):57.
- 1017 21. Roadmap Epigenomics C, Kundaje A, Meuleman W, Ernst J, Bilenky M, Yen  
1018 A, *et al.* Integrative analysis of 111 reference human epigenomes. *Nature.*  
1019 2015;518(7539):317-30.
- 1020 22. Lonsdale J, Thomas J, Salvatore M, Phillips R, Lo E, Shad S, *et al.* The  
1021 Genotype-Tissue Expression (GTEx) project. *Nat Genet.* 2013;45(6):580-5.
- 1022 23. Schierding W, Antony J, Cutfield WS, Horsfield JA, O'Sullivan JM. Intergenic  
1023 GWAS SNPs are key components of the spatial and regulatory network for human  
1024 growth. *Hum Mol Genet.* 2016;25(15):3372-82.
- 1025 24. Fadason T, Schierding W, Lumley T, O'Sullivan JM. Chromatin interactions  
1026 and expression quantitative trait loci reveal genetic drivers of multimorbidities. *Nat*  
1027 *Commun.* 2018;9(1):5198.
- 1028 25. Võsa U, Claringbould A, Westra H-J, Bonder MJ, Deelen P, Zeng B, *et al.*  
1029 Unraveling the polygenic architecture of complex traits using blood eQTL meta-  
1030 analysis. *bioRxiv.* 2018:447367.
- 1031 26. Cruz-Tapias P, Perez-Fernandez OM, Rojas-Villarraga A, Rodriguez-  
1032 Rodriguez A, Arango MT, Anaya JM. Shared HLA Class II in Six Autoimmune  
1033 Diseases in Latin America: A Meta-Analysis. *Autoimmune Dis.* 2012;DOI:  
1034 10.1155/2012/569728.
- 1035 27. Dobbyn A, Huckins LM, Boocock J, Sloofman LG, Glicksberg BS,  
1036 Giambartolomei C, *et al.* Co-localization of Conditional eQTL and GWAS Signatures  
1037 in Schizophrenia. *bioRxiv.* 2017:129429.
- 1038 28. Wen CC, Yee SW, Liang X, Hoffmann TJ, Kvale MN, Banda Y, *et al.* Genome-  
1039 wide association study identifies ABCG2 (BCRP) as an allopurinol transporter and a  
1040 determinant of drug response. *Clin Pharmacol Ther.* 2015;97(5):518-25.

- 1041 29. Kamatani Y, Matsuda K, Okada Y, Kubo M, Hosono N, Daigo Y, *et al.*  
1042 Genome-wide association study of hematological and biochemical traits in a Japanese  
1043 population. *Nat Genet.* 2010;42(3):210-5.
- 1044 30. Matsuo H, Yamamoto K, Nakaoka H, Nakayama A, Sakiyama M, Chiba T, *et*  
1045 *al.* Genome-wide association study of clinically defined gout identifies multiple risk  
1046 loci and its association with clinical subtypes. *Ann Rheum Dis.* 2016;75(4):652-9.
- 1047 31. Bycroft C, Freeman C, Petkova D, Band G, Elliott LT, Sharp K, *et al.* The UK  
1048 Biobank resource with deep phenotyping and genomic data. *Nature.*  
1049 2018;562(7726):203-9.
- 1050 32. Li C, Li Z, Liu S, Wang C, Han L, Cui L, *et al.* Genome-wide association  
1051 analysis identifies three new risk loci for gout arthritis in Han Chinese. *Nat Commun.*  
1052 2015;6:7041.
- 1053 33. Scharpf RB, Mireles L, Yang Q, Kottgen A, Ruczinski I, Susztak K, *et al.* Copy  
1054 number polymorphisms near SLC2A9 are associated with serum uric acid  
1055 concentrations. *BMC Genet.* 2014;15(1):81.
- 1056 34. Wei WH, Guo Y, Kindt AS, Merriman TR, Semple CA, Wang K, *et al.*  
1057 Abundant local interactions in the 4p16.1 region suggest functional mechanisms  
1058 underlying SLC2A9 associations with human serum uric acid. *Hum Mol Genet.*  
1059 2014;23(19):5061-8.
- 1060 35. Kheradpour P, Kellis M. Systematic discovery and characterization of  
1061 regulatory motifs in ENCODE TF binding experiments. *Nucleic Acids Res.*  
1062 2014;42(5):2976-87.
- 1063 36. Shin HJ, Anzai N, Enomoto A, He X, Kim DK, Endou H, *et al.* Novel liver-  
1064 specific organic anion transporter OAT7 that operates the exchange of sulfate  
1065 conjugates for short chain fatty acid butyrate. *Hepatology.* 2007;45(4):1046-55.
- 1066 37. Mandal AK, Mount DB. The molecular physiology of uric acid homeostasis.  
1067 *Annu Rev Physiol.* 2015;77:323-45.

- 1068 38. Nakatochi M, Kanai M, Nakayama A, Hishida A, Kawamura Y, Ichihara S, *et al.*  
1069 *al.* Genome-wide meta-analysis identifies multiple novel loci associated with serum  
1070 uric acid levels in Japanese individuals. *Commun Biol.* 2019;2:115.
- 1071 39. Eckardt KU, Alper SL, Antignac C, Bleyer AJ, Chauveau D, Dahan K, *et al.*  
1072 Autosomal dominant tubulointerstitial kidney disease: diagnosis, classification, and  
1073 management--A KDIGO consensus report. *Kidney Int.* 2015;88(4):676-83.
- 1074 40. Kolz M, Johnson T, Sanna S, Teumer A, Vitart V, Perola M, *et al.* Meta-analysis  
1075 of 28,141 individuals identifies common variants within five new loci that influence  
1076 uric acid concentrations. *PLoS Genet.* 2009;5(6):e1000504.
- 1077 41. Huang W, Shaikh SN, Ganapathy ME, Hopfer U, Leibach FH, Carter AL, *et al.*  
1078 Carnitine transport and its inhibition by sulfonylureas in human kidney proximal  
1079 tubular epithelial cells. *Biochem Pharmacol.* 1999;58(8):1361-70.
- 1080 42. Bachhawat AK, Yadav S. The glutathione cycle: Glutathione metabolism  
1081 beyond the gamma-glutamyl cycle. *IUBMB Life.* 2018;70(7):585-92.
- 1082 43. Wang CK, Yang SC, Hsu SC, Chang FP, Lin YT, Chen SF, *et al.* CHAC2 is  
1083 essential for self-renewal and glutathione maintenance in human embryonic stem cells.  
1084 *Free Radic Biol Med.* 2017;113:439-51.
- 1085 44. Frey IM, Rubio-Aliaga I, Siewert A, Sailer D, Drobyshev A, Beckers J, *et al.*  
1086 Profiling at mRNA, protein, and metabolite levels reveals alterations in renal amino  
1087 acid handling and glutathione metabolism in kidney tissue of *Pept2*<sup>-/-</sup> mice. *Physiol*  
1088 *Genomics.* 2007;28(3):301-10.
- 1089 45. Bahn A, Hagos Y, Reuter S, Balen D, Brzica H, Krick W, *et al.* Identification  
1090 of a new urate and high affinity nicotinate transporter, hOAT10 (SLC22A13). *J Biol*  
1091 *Chem.* 2008;283(24):16332-41.
- 1092 46. Giri AK, Banerjee P, Chakraborty S, Kauser Y, Undru A, Roy S, *et al.* Genome  
1093 wide association study of uric acid in Indian population and interaction of identified  
1094 variants with Type 2 diabetes. *Sci Rep.* 2016;6:21440.



- 1095 47. Houang EM, Sham YY, Bates FS, Metzger JM. Muscle membrane integrity in  
1096 Duchenne muscular dystrophy: recent advances in copolymer-based muscle membrane  
1097 stabilizers. *Skelet Muscle*. 2018;8(1):31.
- 1098 48. Albrecht DE, Sherman DL, Brophy PJ, Froehner SC. The ABCA1 cholesterol  
1099 transporter associates with one of two distinct dystrophin-based scaffolds in Schwann  
1100 cells. *Glia*. 2008;56(6):611-8.
- 1101 49. Haenggi T, Schaub MC, Fritschy JM. Molecular heterogeneity of the  
1102 dystrophin-associated protein complex in the mouse kidney nephron: differential  
1103 alterations in the absence of utrophin and dystrophin. *Cell Tissue Res*.  
1104 2005;319(2):299-313.
- 1105 50. Mandal AK, Mercado A, Foster A, Zandi-Nejad K, Mount DB. Uricosuric  
1106 targets of tranilast. *Pharmacol Res Perspect*. 2017;5(2):e00291.
- 1107 51. Riedmaier AE, Burk O, van Eijck BAC, Schaeffeler E, Klein K, Fehr S, *et al*.  
1108 Variability in hepatic expression of organic anion transporter 7/SLC22A9, a novel  
1109 pravastatin uptake transporter: impact of genetic and regulatory factors.  
1110 *Pharmacogenomics J*. 2016;16(4):341-51.
- 1111 52. Mattila J, Havula E, Suominen E, Teesalu M, Surakka I, Hynynen R, *et al*.  
1112 Mondo-Mlx Mediates Organismal Sugar Sensing through the Gli-Similar Transcription  
1113 Factor Sugarbabe. *Cell reports*. 2015;13(2):350-64.
- 1114 53. Ortega-Prieto P, Postic C. Carbohydrate Sensing Through the Transcription  
1115 Factor ChREBP. *Front Genet*. 2019;10:472.
- 1116 54. Stoltzman CA, Peterson CW, Breen KT, Muoio DM, Billin AN, Ayer DE.  
1117 Glucose sensing by MondoA: Mlx complexes: a role for hexokinases and direct  
1118 regulation of thioredoxin-interacting protein expression. *Proc Natl Acad Sci U S A*.  
1119 2008;105(19):6912-7.
- 1120 55. Gosling AL, Boocock J, Dalbeth N, Harre Hindmarsh J, Stamp LK, Stahl EA,  
1121 *et al*. Mitochondrial genetic variation and gout in Maori and Pacific people living in  
1122 Aotearoa New Zealand. *Ann Rheum Dis*. 2018;77(4):571-8.

- 1123 56. Menezes MJ, Guo Y, Zhang J, Riley LG, Cooper ST, Thorburn DR, *et al.*  
1124 Mutation in mitochondrial ribosomal protein S7 (MRPS7) causes congenital  
1125 sensorineural deafness, progressive hepatic and renal failure and lactic acidemia. *Hum*  
1126 *Mol Genet.* 2015;24(8):2297-307.
- 1127 57. Dogra R, Bhatia R, Shankar R, Bansal P, Rawal RK. Enasidenib: First Mutant  
1128 IDH2 Inhibitor for the Treatment of Refractory and Relapsed Acute Myeloid Leukemia.  
1129 *Anticancer Agents Med Chem.* 2018;18(14):1936-51.
- 1130 58. Amary MF, Damato S, Halai D, Eskandarpour M, Berisha F, Bonar F, *et al.*  
1131 Ollier disease and Maffucci syndrome are caused by somatic mosaic mutations of IDH1  
1132 and IDH2. *Nat Genet.* 2011;43(12):1262-5.
- 1133 59. Consortium GP. A global reference for human genetic variation. *Nature.*  
1134 2015;526(7571):68-74.
- 1135 60. Yang J, Lee SH, Goddard ME, Visscher PM. GCTA: a tool for genome-wide  
1136 complex trait analysis. *Am J Hum Genet.* 2011;88(1):76-82.
- 1137 61. Bulik-Sullivan BK, Loh PR, Finucane HK, Ripke S, Yang J, Schizophrenia  
1138 Working Group of the Psychiatric Genomics C, *et al.* LD Score regression distinguishes  
1139 confounding from polygenicity in genome-wide association studies. *Nat Genet.*  
1140 2015;47(3):291-5.
- 1141 62. Yang J, Ferreira T, Morris AP, Medland SE, Genetic Investigation of ATC,  
1142 Replication DIG, *et al.* Conditional and joint multiple-SNP analysis of GWAS  
1143 summary statistics identifies additional variants influencing complex traits. *Nat Genet.*  
1144 2012;44(4):369-75, S1-3.
- 1145 63. Gao XY, Stamier J, Martin ER. A multiple testing correction method for genetic  
1146 association studies using correlated single nucleotide polymorphisms. *Genet epidemiol.*  
1147 2008;32(4):361-9.
- 1148 64. Finucane HK, Bulik-Sullivan B, Gusev A, Trynka G, Reshef Y, Loh PR, *et al.*  
1149 Partitioning heritability by functional annotation using genome-wide association  
1150 summary statistics. *Nat Genet.* 2015;47(11):1228.

- 1151 65. Benjamini Y, Hochberg Y. Controlling the False Discovery Rate - a Practical  
1152 and Powerful Approach to Multiple Testing. *J R Stat Soc B*. 1995;57(1):289-300.
- 1153 66. Wickham H. *ggplot2: elegant graphics for data analysis*: Springer; 2016.
- 1154 67. Kichaev G, Roytman M, Johnson R, Eskin E, Lindstrom S, Kraft P, *et al*.  
1155 Improved methods for multi-trait fine mapping of pleiotropic risk loci. *Bioinformatics*.  
1156 2017;33(2):248-55.
- 1157 68. Giambartolomei C, Vukcevic D, Schadt EE, Franke L, Hingorani AD, Wallace  
1158 C, *et al*. Bayesian Test for Colocalisation between Pairs of Genetic Association Studies  
1159 Using Summary Statistics. *Plos Genetics*. 2014;10(5):e1004383.
- 1160 69. Fadason T, Ekblad C, Ingram JR, Schierding WS, O'Sullivan JM. Physical  
1161 Interactions and Expression Quantitative Traits Loci Identify Regulatory Connections  
1162 for Obesity and Type 2 Diabetes Associated SNPs. *Front Genet*. 2017;8:150.
- 1163 70. Rao SS, Huntley MH, Durand NC, Stamenova EK, Bochkov ID, Robinson JT,  
1164 *et al*. A 3D map of the human genome at kilobase resolution reveals principles of  
1165 chromatin looping. *Cell*. 2014;159(7):1665-80.
- 1166 71. GTEx Consortium. The Genotype-Tissue Expression (GTEx) project. *Nat*  
1167 *Genet*. 2013;45(6):580-5.
- 1168 72. Cadzow M, Merriman TR, Dalbeth N. Performance of gout definitions for  
1169 genetic epidemiological studies: analysis of UK Biobank. *Arthritis Res Ther*.  
1170 2017;19(1):181.
- 1171 73. Liman ER, Tytgat J, Hess P. Subunit stoichiometry of a mammalian K<sup>+</sup> channel  
1172 determined by construction of multimeric cDNAs. *Neuron*. 1992;9(5):861-71.
- 1173

1174 **Supporting Information**

1175 **Supplementary Figure 1. Q-Q plots for serum urate.**

1176 Quantile-quantile plot showing observed P-values versus expected P-values. Q-Q  
1177 curves are provided for: all SNPs, excluding highly significant loci ( $P < 1E-20$ ), and  
1178 excluding GWAS significant loci ( $P < 5E-08$ ). Genomic-control is provided with and  
1179 without the ImpG imputed SNPs. The LD-score intercept is provided for the European  
1180 and East Asian GWAS.

1181

1182 **Supplementary Figure 2. Regional associations plot of the 3 undescribed serum  
1183 urate loci identified in the Okada *et al.* East Asian GWAS.**

1184 Regional association plots of the 3 previously undescribed Chr11 serum urate loci  
1185 (*SLC22A9*, *PLA2G16* and *AIP*) that were identified in the East Asian GWAS. The lead  
1186 SNPs are indicated by a purple dot. The color of the surrounding SNPs indicates the  
1187 strength of LD with the lead SNP according to the key in the left top hand corner,  
1188 measured as  $r^2$  found in the HapMap data (hg19/1000 genomes Nov 2014) East Asian.  
1189 The plots were generated using LocusZoom.

1190

1191 **Supplementary Figure 3. Regional association plots for the 7 novel serum urate  
1192 loci identified in the trans-ancestral meta-analysis.**

1193 Regional association plots of the 7 novel serum urate loci (*FGF*, *LINC00603*, *HLA-*  
1194 *DQB1*, *B4GALT1*, *BICC1*, *FLRT1* and *USP2*) that were identified by trans-ancestral  
1195 meta-analysis. The lead SNPs are indicated by a purple dot. The color of the  
1196 surrounding SNPs indicates the strength of LD with the lead SNP according to the key  
1197 in the left top hand corner, measured as  $r^2$  found in the HapMap data (hg19/1000  
1198 genomes Nov 2014). European LD data were utilized as the reference for the trans-  
1199 ancestral regional association plots. The plots were generated using LocusZoom.

1200

1201 **Supplementary Figure 4. Regional association plot of the *RELA* locus reveals an  
1202 East Asian specific association with serum urate levels.**

1203 Regional association plots at the *RELA* locus for both the European and East Asian  
1204 GWAS are shown. The lead SNPs are indicated by a purple dot. The color of the  
1205 surrounding SNPs indicates the strength of LD with the lead SNP according to the key  
1206 in the left top hand corner, measured as  $r^2$  found in the HapMap data (hg19/1000  
1207 genomes Nov 2014). a) Regional association plot with LD calculated from the index

1208 European SNP variant *rs12289836*. b) Regional association plot with LD calculated  
1209 from the East Asian specific variant *rs1227200*. The plots were generated using  
1210 LocusZoom.

1211

1212 **Supplementary Figure 5. Regional association plots of all significant ( $P < 5E-08$ )**  
1213 **serum urate loci.**

1214 For each locus, we have provided regional association plots for the East Asian and  
1215 European GWAS in addition to the trans-ancestral GWAS. The lead SNPs are indicated  
1216 by a purple dot. The color of the surrounding SNPs indicates the strength of LD with  
1217 the lead SNP according to the key in the left top hand corner, measured as  $r^2$  found in  
1218 the HapMap data (hg19/1000 genomes Nov 2014). European LD data were utilized as  
1219 the reference for the trans-ancestral regional association plots. The plots were generated  
1220 using LocusZoom.

1221

1222 **Supplementary Figure 6. Regional association plot of the *MAF* locus reveals an**  
1223 **East Asian-specific association and a shared association with serum urate levels.**

1224 Regional association plots at the *MAF* locus from both the European and East Asian  
1225 serum urate GWAS are shown. The lead SNPs are indicated by a purple dot. The color  
1226 of the surrounding SNPs indicates the strength of LD with the lead SNP according to  
1227 the key in the left top hand corner, measured as  $r^2$  found in the HapMap data (hg19/1000  
1228 genomes Nov 2014). (A) Regional association plot with LD calculated from the shared  
1229 trans-ancestral variant *rs1150189*. (B) Regional association plot with LD calculated  
1230 from the East Asian-specific variant *rs889472*. The plots were generated using  
1231 LocusZoom.

1232

1233 **Supplementary Figure 7. Regional association plots of eQTL colocalization.**

1234 For each locus, regional association plots for the serum urate locus (European GWAS)  
1235 and the GTEx eQTL results are shown. For any gene that colocalized with a serum  
1236 urate locus in multiple-tissues, we only show one representative figure pair. For serum  
1237 urate loci with multiple colocalized genes, we show one representative figure pair for  
1238 each colocalized gene. The lead SNPs are indicated by a purple dot. The color of the  
1239 surrounding SNPs indicates the strength of LD with the lead SNP according to the key  
1240 in the left top hand corner, measured as  $r^2$  found in the European HapMap data  
1241 (hg19/1000 genomes Nov 2014). The plots were generated using LocusZoom.

1242

1243 **Supplementary Figure 8. Regional association plots of the *DMD* and *UTRN* loci.**

1244 Regional association plots at *UTRN* (LD calculated from lead SNP rs4896735 using  
1245 European LD from 1000 genomes 2014) from the European urate GWAS and *DMD*  
1246 from the Japanese urate GWAS (LD calculated from lead SNP rs171843 using Asian  
1247 LD from 1000 genomes 2014) are shown. The plot was generated using LocusZoom.

1248

1249 **Supplementary Figure 9. Cell type-specific functional heritability enrichments.**

1250 Cell type-specific enrichments for serum urate levels. The color of each bar represents  
1251 the cell type group of each annotation. The direction of enrichment is indicated by  
1252 adding a sign to the  $-\log_{10}$  P-value. A positive sign indicates enrichment and a negative  
1253 sign indicates depletion. These results are displayed in four panels one for each histone  
1254 mark: a) H3K27ac ChIP-seq; b) H3K9ac; c) H3K4me3; d) H3K4me1.

1255

1256 **Supplementary Figure 10. Regional association plots of *RP11-448G15.1* and**

1257 ***RNF169* eQTL.** For each locus, regional association plots for the serum urate locus  
1258 (European GWAS) and the GTEx eQTL results are shown. The lead SNPs are indicated  
1259 by a purple dot. The color of the surrounding SNPs indicates the strength of LD with  
1260 the lead SNP according to the key in the left top hand corner, measured as  $r^2$  found in  
1261 the European HapMap data (hg19/1000 genomes Nov 2014). The plots were generated  
1262 using LocusZoom.

1263

1264 **Supplementary Table 1. Partitioned serum urate heritability enrichment**  
1265 **estimates for cell-type groups.** These enrichments were generated using LD-score  
1266 functional partitioning of the European GWAS summary statistics.

1267

1268 **Supplementary Table 2. Partitioned serum urate heritability enrichment**  
1269 **estimates for cell-type specific epigenomic profiles.** These enrichments were  
1270 generated using LD-score functional partitioning of the European GWAS summary  
1271 statistics.

1272

1273 **Supplementary Table 3. PAINTOR results.** Trans-ancestral functional fine-mapping  
1274 results for 36 serum urate loci (excluding *MHC* and *RELA*). Loci can be distinguished  
1275 by their index SNP and locus names. The results are summarized from three PAINTOR  
1276 models: the model which used the GWAS data from both the East Asian and European  
1277 population, the model which used the GWAS data from the East Asian population only,

1278 and the model which used the GWAS data from the European population only. All  
1279 models included significant cell type group annotations.

1280

1281 **Supplementary Table 4. Functionally annotated variants identified by PAINITOR.**

1282 Haploreg v4.1 was used to annotate all variants with a PAINITOR posterior probability  
1283 > 0.8. Annotations include enhancer histone marks, DNase peaks, proteins bound  
1284 (ChIP), motifs changed by the alternate allele, number of GWAS and eQTL hits and  
1285 location with respect to the nearest gene.

1286